

Axionlike particles searches in reactor experiments

D. Aristizabal Sierra,^{a,b} V. De Romeri,^c L. J. Flores,^d D.K. Papoulias^e

^a*Universidad Técnica Federico Santa María - Departamento de Física Casilla 110-V, Avda. España 1680, Valparaíso, Chile*

^b*IFPA, Dep. AGO, Université de Liège, Bat B5, Sart Tilman B-4000 Liège 1, Belgium*

^c*Instituto de Física Corpuscular, CSIC/Universitat de València, Calle Catedrático José Beltrán, 2 E-46980 Paterna, Spain*

^d*Instituto de Física, Universidad Nacional Autónoma de México, A.P. 20-364, Ciudad de México 01000, México*

^e*Department of Physics, University of Ioannina GR-45110 Ioannina, Greece*

E-mail: daristizabal@ulg.ac.be, deromeri@ific.uv.es,
luisjf89@fisica.unam.mx, d.papoulias@uoi.gr

ABSTRACT: Reactor neutrino experiments provide a rich environment for the study of axionlike particles (ALPs). Using the intense photon flux produced in the nuclear reactor core, these experiments have the potential to probe ALPs with masses below 10 MeV. We explore the feasibility of these searches by considering ALPs produced through Primakoff and Compton-like processes as well as nuclear transitions. These particles can subsequently interact with the material of a nearby detector via inverse Primakoff and inverse Compton-like scatterings, via axio-electric absorption, or they can decay into photon or electron-positron pairs. We demonstrate that reactor-based neutrino experiments have a high potential to test ALP-photon couplings and masses, currently probed only by cosmological and astrophysical observations, thus providing complementary laboratory-based searches. We furthermore show how reactor facilities will be able to test previously unexplored regions in the \sim MeV ALP mass range and ALP-electron couplings of the order of $g_{aee} \sim 10^{-8}$ as well as ALP-nucleon couplings of the order of $g_{ann}^{(1)} \sim 10^{-9}$, testing regions beyond TEXONO and Borexino limits.

Contents

1	Introduction	1
2	Axionlike particle interactions	3
3	ALPs production and detection mechanisms at reactors	5
3.1	Production and detection through photon-ALP coupling	9
3.2	Production and detection through electron-ALP coupling	14
3.3	Production through nucleon-ALP coupling	16
4	Experimental sensitivities	20
5	Conclusions	30

1 Introduction

In recent years there has been an increasing interest in weakly/feebly coupled light physics. Arguably the main motivation has been given by searches at the LHC, which have provided null results of new physics at the TeV scale. Weakly coupled hidden sectors are a rather plausible explanation for the absence of such signals. They are motivated as well by the fact that the absence of dark matter direct detection signals can be justified if the new secluded sector involves sub-MeV degrees of freedom. A common feature of these scenarios is the presence of light scalars/pseudoscalars, usually called axionlike particles (ALPs), with masses and couplings to Standard Model (SM) particles which can span over many orders of magnitude. Examples of the latter are QCD axions [1–4], a widely explored extension of the SM addressing the strong CP problem. They can also arise as a consequence of spontaneously broken approximate symmetries, of which examples include familons and Majorons [5–7]. In these scenarios, ALPs are the pseudo-Nambu-Goldstone bosons of theories where a symmetry group $G \supset SU(3) \times SU(2) \times U(1)$ is spontaneously broken at a high scale, leaving behind light (pseudo)scalar states.

ALPs may generate signals in a large variety of experimental environments. They can as well affect the evolution of stars and of core-collapse supernova explosions and can potentially affect the early universe dynamics. They can, for instance, contribute to the number of relativistic degrees of freedom or they can release entropy in the heat bath thus disrupting BBN predictions (see e.g. [8, 9] and references therein). In the high-mass regime, and at the laboratory level, ALPs have been searched for in

beam-dump experiments as well as in radiative Υ decays at CLEO and BaBar [10–15]. They have been as well investigated at accelerator experiments through different event topologies, first at LEP and more recently at the LHC [16–19]. Prospects of exploring regions not yet tested in this mass regime include Belle II, NA62, NA64, SeaQuest, MATHUSLA, CODEX-b, FASER and SHiP [20–28].

ALPs have been searched for as well in reactor experiments, motivated by theoretical arguments pointed out first by Weinberg and subsequently by Donnelly, Freedman, Lytel, Peccei and Schwartz [3, 29]¹. To the best of our knowledge, ALP reactor searches looking for various nuclear magnetic transitions were pioneered at the Bugey reactor [30], and followed by searches carried out by Zehnder and Lehmann et. al. in which instead ALPs were searched for in nuclear magnetic transitions of $^{127}\text{Ba}^*$ and $^{65}\text{Cu}^*$ [31, 32]. Most recently, the TEXONO collaboration extended the analysis of Ref. [30] through a comprehensive investigation at the Kuo-Sheng reactor nuclear power plant, by also employing nuclear magnetic transitions along with inverse Compton-like and Primakoff scattering for detection [33].

At present, there is a rapidly developing physics program aiming at measuring coherent elastic neutrino-nucleus scattering ($\text{CE}\nu\text{NS}$) using reactor neutrinos, which offers exciting possibilities to explore physics beyond the SM. To this purpose, several new experiments with sub-keV threshold capabilities are in preparation in The Americas, Western and Eastern Europe and Asia, including—but not limited to—CONNIE, MINER, CONUS, ν -cleus, Ricochet, RED-100 and TEXONO [34–40] (for a detailed review see Ref. [41]). Apart from $\text{CE}\nu\text{NS}$ measurements, this program is aiming at improving upon previous measurements of the weak mixing-angle, the root-mean-square radii of neutron distributions for different isotopes, as well as to look for new physics signatures in the form of e.g. neutrino magnetic moments, light vector and scalar mediators and neutrino generalized interactions (see e.g. [42–54]). Recently, it has been pointed out that these technologies also open up a new direction for ALP searches [55], further motivating our present work.

In this paper, we investigate the feasibility and extent of such searches by including leading ALP production and detection mechanisms at reactor neutrino experiments. In addition to nuclear magnetic transitions, considered by previous reactor searches, here we take into account additional ALP production mechanisms such as Compton-like and Primakoff scattering. We furthermore consider detection through their inverse processes as well as via axio-electric absorption and ALP decays to diphoton and electron pairs.

Our analysis follows minimal ALP assumptions in the sense that it considers only those processes that allow production and detection through the same ALP-SM coupling, the exception being production through nuclear de-excitation. In this

¹These arguments were applicable to the QCD axion and so these searches. The experimental results, however, hold as well for ALPs.

case we consider detection through either ALP-photon or ALP-electron couplings, following to a large extent the analysis carried out by TEXONO in Ref. [33]. Rather than sticking to a particular CE ν NS reactor-based experiment, our analysis is formulated as generic as possible, and therefore being representative of what current or near-future technologies could achieve.

Due to kinematic constraints, reactor-based searches will cover regions up to ALP masses of order of 10 MeV. Thus they will not cover some of the regions that Belle II, NA62, NA64, SeaQuest, MATHUSLA, CODEX-b, FASER and SHiP will have access to. However they can potentially provide valuable information on regions yet unexplored by laboratory experiments, while in some cases they can actually explore regions so far not tested at all. Since CE ν NS reactor experiments will run anyway, an ALP research program will serve towards widening the physics reach of these facilities in a direction complementary to other ALP search strategies.

The remainder of this paper is organized as follows. In Sec. 2 we present the interactions our analysis deals with and we briefly discuss some representative QCD axion models. In Sec. 3 we discuss the ALPs production and detection mechanisms considered in the present study, relevant at reactor experiments. In Sec. 4 we present our main results, the sensitivities achievable in ongoing or near-future experiments, along with sensitivities expected at the next-generation CE ν NS reactor experiments. Finally, in Sec. 5 we summarize and present our conclusions.

2 Axionlike particle interactions

Axionlike particles (ALP) are pseudoscalars that feebly couple to the SM particles. They arise in a variety of new physics scenarios, including those related with dark matter in which the pseudoscalar mediates interactions between the dark and visible sectors [56, 57]. In general, they can be expected in scenarios where the spontaneous breaking of a global symmetry takes place. In that regard, the Majoron could be thought as a prototypical example linked to spontaneous lepton number symmetry breaking, and ultimately with the origin of Majorana neutrino masses [58]. From a more theoretical point of view, they can be as well understood as low energy manifestations of string theories [59, 60].

Strictly speaking, the SM degrees of freedom to which the ALPs couple depend on the specific model realization. However, from a purely phenomenological point of view the ALP couplings can be parameterized in terms of dimension-five effective operators. Here we consider couplings to photons, electrons and nucleons, for which the interactions can be written according to

$$\mathcal{L} = \mathcal{L}_a - \frac{1}{4} g_{a\gamma\gamma} a F_{\mu\nu} \tilde{F}^{\mu\nu} - i g_{aee} a \bar{e} \gamma_5 e - i a \bar{n} \gamma_5 (g_{ann}^{(0)} + \tau_3 g_{ann}^{(1)}) n, \quad (2.1)$$

where n refers to the proton-neutron isospin doublet and $g_{ann}^{(0)}$ ($g_{ann}^{(1)}$) to the isosinglet (isotriplet) axion-nucleon couplings, while the first term in the Lagrangian involves the ALP kinetic and mass terms as well as the scalar potential.

It is worth noting that the dimension-five operator nature of the couplings to photons is evident, while for fermions this is not the case. Indeed, couplings to fermions are dictated by derivative interactions (see e.g. [8, 9])

$$\mathcal{L}_f = \frac{C_{af}}{2f_a} \bar{f} \gamma_5 \gamma^\mu f \partial_\mu a \quad (f = e, p, n) , \quad (2.2)$$

with f_a the ALP decay constant and C_{af} dimensionless strength couplings. Operators in the Lagrangian (2.2) are of dimension five, but they can be cast into those described in the Lagrangian of Eq. (2.1) with the aid of the fermion equation of motion $\bar{f} \partial_\mu \gamma_5 \gamma^\mu f = -im_f \bar{f} \gamma_5 f$, combined with integration by parts. In terms of the decay constant and fermion masses, the couplings in the Lagrangian (2.2) are thus given by

$$g_{a\gamma\gamma} = \frac{\alpha}{2\pi} \frac{C_{a\gamma}}{f_a} , \quad g_{aff} = m_f \frac{C_{af}}{f_a} . \quad (2.3)$$

So far the discussion applies to ALPs, which are not related with the solution to the strong CP problem and for which their mass and decay constant are not related. Reactor experiments are best suited to test parameter space regions of ALPs rather than of the QCD axion (see Sec. 4). Nevertheless, in what follows we briefly provide a few relations derived in QCD axion models that will enable comparing the extent at which they could be tested (for comprehensive reviews see e.g. [8, 9]). The interactions in (2.1) along with (2.3) hold as well for the QCD axion, but in this case the relation

$$m_a \simeq 5.7 \left(\frac{10^{12} \text{ GeV}}{f_a} \right) \mu\text{eV} \quad (2.4)$$

applies. This expression combined with Eq. (2.3) leads to relations which can be mapped into the axion mass-coupling plane in the form of stripes whose widths depend on the UV completion accounting for the axion effective Lagrangian, namely

$$g_{a\gamma\gamma} = 2.0 \times 10^{-10} C_{a\gamma} \left(\frac{m_a}{\text{eV}} \right) \text{GeV}^{-1} , \quad (2.5)$$

$$g_{aff} = 1.8 \times 10^{-7} C_{af} \left(\frac{m_f}{\text{GeV}} \right) \left(\frac{m_a}{\text{eV}} \right) . \quad (2.6)$$

The dimensionless parameters in Eqs. (2.5) and (2.6) read (see e.g. Ref. [9])

$$C_{a\gamma} = \frac{E}{N} - 1.92 , \quad (2.7)$$

$$C_{ap} = -0.47 + 0.88c_u^0 - 0.39c_d^0 - C_{a,\text{sea}} , \quad (2.8)$$

$$C_{an} = -0.02 + 0.88c_d^0 - 0.39c_u^0 - C_{a,\text{sea}} , \quad (2.9)$$

$$C_{a,\text{sea}} = 0.038c_s^0 + 0.012c_c^0 + 0.009c_b^0 + 0.0035c_t^0 , \quad (2.10)$$

$$C_{ae} = c_e^0 + \frac{3\alpha^2}{4\pi^2} \left[\frac{E}{N} \log \left(\frac{f_a}{m_e} \right) - 1.92 \log \left(\frac{\text{GeV}}{m_e} \right) \right], \quad (2.11)$$

where E and N correspond to the QCD and electromagnetic anomaly coefficients and the second term in Eq. (2.11) arises from one-loop corrections. Barring the case $E/N=0$, the axion couples to (gluons) photons and electrons ($g_{aee} \neq 0$ even for $c_e^0 = 0$). The coefficients c_f^0 are model dependent and in some instances are zero at the tree level.

The most renowned *invisible axion* UV completions are the KSVZ and DFSZ models [61–64], or variants of them. To compare with our sensitivities we select few of them as follows: for KSVZ-type models we consider those with $c_{u_i}^0 = c_{d_i}^0 = c_e^0 = 0$ and $E/N \subset [44/3, 5/3]$, which cover a large variety of hadronic axion models [65]. For the case of DFSZ-type models we instead consider the DFSZ-I and DFSZ-II realizations, for which the relevant parameters are given by

$$\begin{aligned} \text{DSFZ-I: } & \frac{E}{N} = \frac{8}{3}, \quad c_{u_i}^0 = -\frac{1}{3} \cos^2 \beta, \quad c_{d_i}^0 = -\frac{1}{3} \sin^2 \beta, \quad c_{e_i}^0 = -\frac{1}{3} \sin^2 \beta, \\ \text{DSFZ-II: } & \frac{E}{N} = \frac{2}{3}, \quad c_{u_i}^0 = -\frac{1}{3} \cos^2 \beta, \quad c_{d_i}^0 = -\frac{1}{3} \sin^2 \beta, \quad c_{e_i}^0 = \frac{1}{3} \cos^2 \beta, \end{aligned} \quad (2.12)$$

with $\tan \beta = v_u/v_d \in [0.25, 170]$ ($v = \sqrt{v_u^2 + v_d^2} = 246 \text{ GeV}$).

3 ALPs production and detection mechanisms at reactors

Photons are abundantly produced in nuclear power plants. Processes responsible for γ emission are fission, decay of fission products, capture processes in fuel and other materials, inelastic scattering in the fuel, and decay of capture products [66]. The prompt photon flux can be described by

$$\frac{d\Phi_\gamma}{dE_\gamma} = \frac{5.8 \times 10^{17}}{\text{MeV} \cdot \text{sec}} \left(\frac{\text{P}}{\text{MW}} \right) e^{-1.1 E_\gamma/\text{MeV}}, \quad (3.1)$$

an approximation originally derived from an analysis of γ radiation in the FRJ-1 research reactor [67] and which has been recently used in dark photon phenomenological analyses [68, 69].

Once produced, these photons can interact with the fuel material which we assume to be ^{235}U . This choice is motivated by the fact that most of the reactor experiments our analysis applies to, use this uranium isotope (totally or partially) as fuel material. Possible interactions fall in three category processes: (i) a first category with final-state photons, which involves Rayleigh (elastic) or Compton (inelastic) scattering; (ii) a second category that accounts for possible photon absorption by the material, and that involves photo-electric absorption and e -pair production by the nucleus or electron field, (iii) photon-ALP conversion. Specifically, categories (i) and (ii) are SM processes, while category (iii) requires a SM-ALP coupling. The

Experiment	Nuclear Reactor	Power [GW]
TEXONO [40]	Kuo-Sheng Nuclear Power Station	2.9
CONUS [36]	Brokdorf	3.9
ν GeN [70]	Kalinin Nuclear Power Plant	~ 1
MINER [35]	TRIGA 1	10^{-3}
ν CLEUS [37]	FRM2	4
Ricochet [38]	Chooz Nuclear Power Plant	8.54
RED-100 [39]	Kalinin Nuclear Power Plant	~ 1
SBC [71]	ININ (or Laguna Verde)	10^{-3} (1.5)
CONNIE [72]	Angra 2	3.8
ν IOLETA [73]	Atucha II	2
SoLid [74]	BR2	$(0.4, 1) \times 10^{-1}$
NEON [75]	Hanbit Nuclear Power Plant	2.8

Table 1. Reactor neutrino experiments to which our analysis may apply. We also present the associated nuclear reactor along with its thermal power. The color codes are associated with the detection techniques the experiments rely on as specified in Tab. 3.

relevant Feynman diagrams for processes (i) and (ii) are shown in Fig. 1. It is worth noting that processes of type (iii) should involve an initial- and final-state photon and ALP, respectively. Apart from Primakoff photon-ALP conversion (diagram (a) in Fig. 2), the other two proceed from the SM Compton and Rayleigh processes by changing the final-state photon to an ALP (see diagrams (b) and (c) in Fig. 2). The leading mechanisms are Compton-like production and nuclear de-excitation. All these processes involve independent SM-ALP couplings: Primakoff production is enabled by $g_{a\gamma\gamma}$, Compton-like production by g_{aee} and nuclear de-excitation by g_{ann} ($n = \text{neutron, proton}$).

Primakoff, Compton-like and nuclear de-excitation can also serve as detection mechanisms. The other possible detection processes follow from the SM photoelectric absorption and e -pair production by changing $\gamma \rightarrow a$, as shown in Fig. 3. In the former case, axio-electric absorption [76], an ALP is absorbed by an atom resulting in electron emission. In the latter, an ALP is absorbed and an electron-pair is emitted. Depending on the ALP lifetime, detection can proceed as well through ALP decay processes: $a \rightarrow \gamma\gamma$, $a \rightarrow e^+e^-$ and $a \rightarrow nn$ (since for the last two processes $m_a > 2m_e$ and $m_a > 2m_n$ should be satisfied, decay to nucleons is not a viable possibility in nuclear reactor experiments). Table 2 shows the different production and detection mechanisms together with the relevant couplings. From

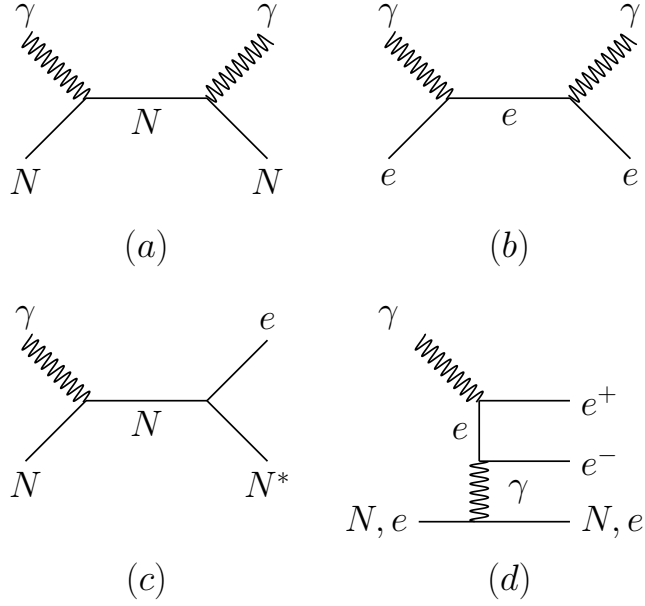


Figure 1. SM photon scattering processes. Process (a) corresponds to elastic scattering (Rayleigh), process (b) to inelastic scattering (Compton), process (c) to photo-electric absorption and process (d) to electron-pair production in the field of the nucleus or electron. Photons produced at the nuclear reactor core can undergo any of these processes when interacting with the reactor fuel.

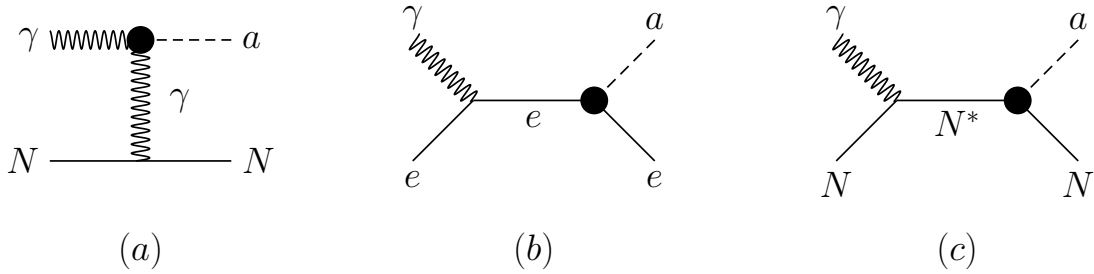


Figure 2. ALPs production mechanisms at a nuclear reactor plant. Process (a) corresponds to Primakoff photon-ALP conversion, process (b) to Compton-like scattering and process (c) to nuclear de-excitation. Depending on the type of SM-ALP coupling (g_{aXX} , $X = \gamma, e, n$, where n refers to nucleons), in addition to the processes shown in Fig. 1, photons interacting with the reactor fuel can be subject to these processes.

this table one can see that *self-contained one-parameter analyses* (axion mass aside) of ALP production should be done as follows:

- Analyses with $g_{a\gamma\gamma}$ should involve production through Primakoff and detection through inverse Primakoff and decay into a γ -pair final states.
- Analyses with g_{aee} should include production through Compton-like and detection through inverse Compton-like, axio-electric, e -pair production in e field and decay into an electron-positron pair final states.

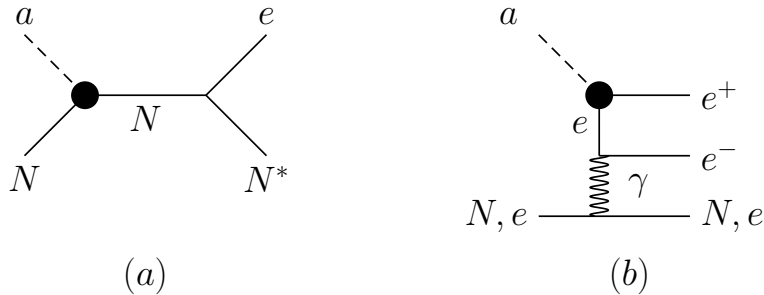


Figure 3. ALPs detection mechanisms, along with inverse Primakoff, inverse Compton-like and nuclear excitation (inverse processes in Fig. 2). Process (a) corresponds to the axio-electric process (photo-electric absorption equivalent, diagram (c) in Fig. 1), while process (b) to axion e -pair production (e -pair production in the field of the nucleus or electron equivalent, diagram (d) in Fig. 1). As in the production case, whether such detection mechanisms are operative depends on the type of coupling the analysis is subject to. See Tab. 2 for details.

- Analyses with g_{ann} should be done considering production through nuclear de-excitation and detection through nuclear excitation.

We relax our analysis from considering ALP e -pair production in the field of N or e^- (diagram (b) in Fig. 3). Although we do not calculate the ALP e -pair production cross sections, we expect that the detection through these processes should produce a rather small event yield, similar to their SM counterparts which are suppressed (see Fig. 4). We do not consider either ALP nuclear excitation in detection. Hence, in our analysis of ALP production through nuclear de-excitation (Sec. 3.3) we consider detection mechanisms which involve other ALP couplings (either g_{aee} or $g_{a\gamma\gamma}$).

Phenomenological ALP studies follow a three-step analysis: (i) production, (ii) propagation towards the detection chamber and (iii) detection. The relevant production mechanisms assumed in the present work, namely, Primakoff conversion, Compton-like scattering or nuclear de-excitation, generate an ALP flux which propagates and can potentially reach the detector depending on the ALP lifetime, determined by its survival probability. Neglecting possible interactions with the detector shielding material, ALPs reaching the detector will then interact with the target material yielding—in principle—a measurable signal. The quantities that intervene in this three-step process then combine through a convolution, that defines the differential event yield from which the number of counts at the detector is calculated.

Possible signals depend on the kind of process ALPs are subject to. For instance, in the axio-electric process ALP absorption by the material produces phonons (from the temperature rise of the absorber) and electron-hole pairs leading to heat and ionization signals. Ideally, detection through the axio-electric process should then be done using dielectric crystals, whose properties are optimized for such type of signatures. DAMA, CDMS and more recently the SuperCDMS Soudan experiment

Scattering processes				
Process		Coupling	Prod	Det
Primakoff	$\gamma + N \leftrightarrow a + N$	$g_{a\gamma\gamma}$	✓	✓
Compton-like	$\gamma + e^- \leftrightarrow a + e^-$	g_{aee}	✓	✓
Nuclear de-excitation	$\gamma + N \leftrightarrow N^* \rightarrow a + N$	g_{ann}	✓	✓
Axio-electric	$a + e^- + Z \rightarrow e^- + Z$	g_{aee}	✗	✓
e -pair production in N	$a + N \rightarrow e^- + e^- + N$	g_{ann}	✗	✓
e -pair production in e	$a + e^- \rightarrow e^- + e^+ + e^-$	g_{aee}	✗	✓
Decay processes				
Process		Coupling	Prod	Det
γ -pair final state	$a \rightarrow \gamma + \gamma$	$g_{a\gamma\gamma}$	✗	✓
e -pair final state	$a \rightarrow e^- + e^+$	g_{aee}	✗	✓
n -pair final state	$a \rightarrow n + n$	g_{ann}	✗	✗

Table 2. ALPs production and detection mechanisms. Check marks (crosses) are used to identify (exclude) production and/or detection processes. Color refers to processes that should be—in principle—included in a self-contained one-parameter analysis. Note that decay to nucleon pairs is forbidden by kinematic arguments.

have followed this strategy, i.e. DAMA using NaI crystals, while CDMS and SuperCDMS Soudan using a cryogenic detector based on high-purity germanium and silicon crystals [77–79]. The different detector technologies as well as detector specifications of typical experiments to which our analysis can apply are shown in Tab. 3. These parameters motivate the generic numbers used in our analysis: germanium as material target, $m_{\text{det}} = 10$ kg and $L = 10$ m (see Sec. 4).

3.1 Production and detection through photon-ALP coupling

Let us now focus on Primakoff-like production and detection processes. In full generality, the determination of the ALP flux involves a convolution (over ingoing photon energies) of the photon flux and the photon-ALP conversion differential cross section, properly normalized to account for the processes (i) and (ii). With the ALP flux at hand, and after assuring the ALP survival probability is sizeable enough, the detection proceeds through a second convolution (over ingoing ALP energies) of the ALP flux and the ALP-photon conversion differential cross section. If the ALP

Detector	Experiment	Material	$m_{\text{det}}[\text{kg}]$	L [m]
Semiconductor detectors (ionization)	TEXONO [40]	Ge	1.06	28
	CONUS [36]	Ge	1	17.1
	ν GeN [70]	Ge	1.6-5	10-12
Low temperature bolometers	MINER [35]	Ge, Si	4	1-2.5
	ν CLEUS [37]	CaWO ₄ , Al ₂ O ₃	10 ⁻²	15-100
	Ricochet [38]	Ge, Zn	10	355/469
Liquid noble-gas detectors (TPC)	RED-100 [39]	Xe	100	19
	SBC [71]	LAr, Xe	10	3/30
CCD	CONNIE [72]	Si	~ 0.05	30
	ν IOLETA [73]	Si	1	12
Scintillators	SoLid [74]	⁶ LiF : ZnS(Ag)	1600	~ 7.6
	NEON [75]	NaI[Tl]	3.3-10	24

Table 3. Detectors to which our analysis may apply, along with relevant parameters for ALP detection. With germanium as a target material, $m_{\text{det}} = 10\text{kg}$ and $L = 10\text{m}$ are rather representative of the experiments our analysis can cover. CCD refers to charge-coupled devices.

undergoes decay within the detector chamber, photon signals can be triggered as well by its decay. In such a scenario the ALP detection is therefore a combination of inverse-Primakoff scattering and decay contributions, with the latter being mainly relevant in the “high” ALP mass region (the decay partial width is proportional to the ALP mass). Let us discuss this in more detail.

Accounting for the probability that an ALP of energy E_a is emitted after a $\gamma - ^{235}\text{U}$ interaction, the ALP flux proceeds then from the following convolution

$$\frac{d\Phi_a^{\text{P}}}{dE_a} = \mathcal{P}_{\text{surv}} \int_{E_{\gamma',\text{min}}}^{E_{\gamma',\text{max}}} \frac{1}{\sigma_{\text{Tot}}} \frac{d\sigma_{\text{P}}^{\text{P}}(E_{\gamma'}, E_a)}{dE_a} \frac{d\Phi_{\gamma'}}{dE_{\gamma'}} dE_{\gamma'}, \quad (3.2)$$

where $\sigma_{\text{Tot}} = \sigma_{\text{SM}} + \sigma_{\text{P}}^{\text{P}}$, with the SM cross section being $\sigma_{\text{SM}} = \sigma_{\text{R}} + \sigma_{\text{C}} + \sigma_{\text{PE}} + \sigma_{e\text{-pair}}$, while $\sigma_{\text{P}}^{\text{P}} \equiv \sigma_{\gamma \rightarrow a}$ is the total Primakoff scattering cross section for ALP production. Results for the SM components are obtained from the XCOM: Photon cross section database [80] and shown in Fig. 4 for completeness. The integration

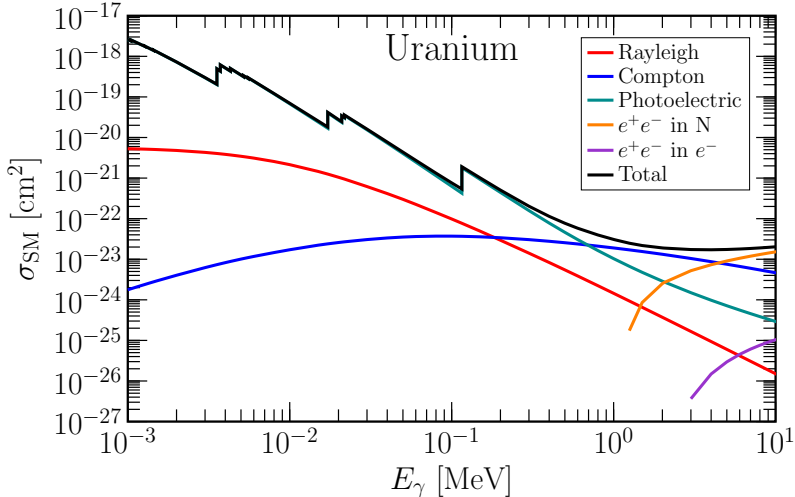


Figure 4. SM photon cross sections for uranium taken from the XCOM photon cross section database [80].

limits are determined by the kinematic relation ²

$$E_{\gamma'} = \frac{2E_a M_N - m_a^2}{2(M_N - E_a + |\vec{p}_a| \cos \theta)} , \quad (3.3)$$

with $E_{\gamma'}^{\min}$ ($E_{\gamma'}^{\max}$) found for $\cos \theta = +1$ ($\cos \theta = -1$) and M_N being the nuclear mass. Differences between the upper and lower limits are in the sub-keV ballpark, almost independent of the ALP mass. Kinematically, this implies that a photon with a given energy $E_{\gamma'}$ produces ALPs within a rather narrow energy range.

The ALP survival probability, assuring that the ALP flux reaches the detector, can be cast as [55]

$$\mathcal{P}_{\text{surv}} = e^{-LE_a/|\vec{p}_a|\tau} , \quad (3.4)$$

where L refers to the distance between the reactor and detector and τ to the ALP lifetime in the fixed target frame, determined in turn by the ALP total decay width: $\tau^{-1} = \Gamma_{a \rightarrow 2\gamma} \times m_a/E_a$, while the decay width reads

$$\Gamma_{a \rightarrow 2\gamma} \equiv \Gamma(a \rightarrow \gamma\gamma) = \frac{g_{a\gamma\gamma}^2 m_a^3}{64\pi} . \quad (3.5)$$

Thus, for a photon with energy $E_{\gamma'}$ the consequent ALP distribution can be

²To avoid confusion, throughout the manuscript the incident and outgoing photon energies are denoted by $E_{\gamma'}$ and E_γ , respectively.

approximated with a monochromatic one ³

$$\frac{d\sigma_P^P}{dE_a} \simeq \sigma_P^P(E_a)\delta(E_{\gamma'} - E_a) . \quad (3.6)$$

This observation allows to determine the ALP flux with a simplified version of Eq. (3.2), namely

$$\frac{d\Phi_a^P}{dE_a} = \frac{\sigma_P^P}{\sigma_{\text{Tot}}} \left. \frac{d\Phi_{\gamma'}}{dE_{\gamma'}} \right|_{E_{\gamma'}=E_a} . \quad (3.7)$$

For the calculation of the total Primakoff scattering cross section we rely on the expression [81]

$$\frac{d\sigma_P^P}{dt} = 2\alpha Z^2 F^2(t) g_{a\gamma\gamma}^2 \frac{M_N^4}{t^2(M_N^2 - s)^2(t - 4M_N^2)^2} \left\{ m_a^2 t(M_N^2 + s) - m_a^4 M_N^2 - t[(M_N^2 - s)^2 + st] \right\} , \quad (3.8)$$

a result that does not involve any approximation (see discussion below). Here s, t are Mandelstam variables and $\alpha Z^2 F^2(t)$ is the effective electric charge to which the photon couples to. Its value is controlled by $F^2(t)$, a form factor that we normalize to unity. For a sufficiently small exchanged momentum $|q| = \sqrt{-t} \leq \sqrt{7.39m_e^2} \simeq 7.0 \times 10^{-3} \text{ fm}^{-1}$, the DeBroglie wavelength of the scattering process is large enough so to partially involve the atomic electron cloud [82]. In that case the effective electric charge is diminished (screened), with the reduction depending on how small the exchanged momentum becomes. For such regime we use the following atomic form factor [83]

$$F_{\text{Atomic}}^2(t) = \left(\frac{a_0^2 t}{1 - a_0^2 t} \right)^2 , \quad (3.9)$$

with a_0 calculated in the Thomas-Fermi atom using the Moliere representation

$$a_0 = \frac{184.15}{\sqrt{2.718}} \frac{1}{Z^{1/3} m_e} . \quad (3.10)$$

Since we choose $t = q^2 < 0$, contrary to what Ref. [83] does, Eq. (3.9) results from shifting $t \rightarrow -t$ in the form factor provided by that reference. For a larger exchanged momentum $|q| = \sqrt{-t} > \sqrt{7.39m_e^2} \simeq 7.0 \times 10^{-3} \text{ fm}^{-1}$ the DeBroglie wavelength becomes smaller and hence the atomic electron cloud is not relevant anymore. However as q increases the nuclear electric charge diminishes as well,

³For definiteness, in what follows the cross sections are written in the form σ_X^Y , where $X = (\text{P}, \text{D})$ indicates the corresponding mechanism e.g. production or detection and $Y = (\text{P}, \text{C}, \text{A})$ indicates the nature of the process e.g. Primakoff-like, Compton-like and axio-electric, respectively. Similarly, the ALP flux is given in the form $\frac{d\Phi_a^Z}{dE_a}$, where $Z = (\text{P}, \text{C}, \text{MT})$ accounts for Primakoff-, Compton- and Magnetic Transition (MT)-induced ALPs, while the number of events is written in the form \mathcal{N}_Y^Z .

therefore the atomic form factor has to be replaced by a nuclear form factor which we choose to be of the Helm form [84]⁴. It is worth emphasizing that while the inclusion of a nuclear form factor has a negligible effect on our results, the inclusion of the atomic form factor is instead important, in particular in the low ALP mass region $m_a \lesssim 10^4$ eV. This can be understood from the nature of the Primakoff process, for which the largest amount of events are found at small t or along the forward direction.

The calculation of the Primakoff cross section in Ref. [82] is valid in the forward scattering limit as well as in the limit $E_\gamma = E_a$ and $m_a \rightarrow 0$. In contrast, the result in Eq. (3.8) does not involve any of those approximations, even if $E_\gamma = E_a$ is still valid to a large degree, as we have already pointed out. However, departures from forward scattering as well as a massive ALP can produce sizable deviations, particularly relevant at photon energy threshold⁵.

For the integration of the Primakoff differential cross section in Eq. (3.6) we use the following limits [85]

$$t_{\max}(t_{\min}) = \frac{m_a^4}{4s} - (p_{1\text{cm}} \mp k_{1\text{cm}})^2, \quad (3.11)$$

where p_1 (k_1) refer to the initial-state photon (final-state axion) three-momentum given by

$$p_{1\text{cm}} = \frac{s - M_N^2}{2\sqrt{s}}, \quad k_{1\text{cm}} = \left[\frac{(s + m_a^2 - M_N^2)^2}{4s} - m_a^2 \right]^{1/2}, \quad (3.12)$$

with $s = M_N^2 + 2M_N E_{\gamma'}$.

Then, the differential event rate consists of two terms, one from the inverse-Primakoff scattering and another one from ALP decays $a \rightarrow \gamma\gamma$

$$\frac{d\mathcal{N}_{\text{Tot}}^{\text{P}}}{dE_a} = \frac{d\mathcal{N}_{\text{P}}^{\text{P}}}{dE_a} + \frac{d\mathcal{N}_{\text{decay}}^{\text{P}}}{dE_a}. \quad (3.13)$$

Here, the first term results from a convolution of the ALP flux and the ALP-photon differential cross section⁶, namely

$$\frac{d\mathcal{N}_{\text{P}}^{\text{P}}}{dE_a} = m_{\text{det}} \frac{N_T \Delta t}{4\pi L^2} \int \frac{d\Phi_a^{\text{P}}}{dE_a} \frac{d\sigma_D^{\text{P}}}{dE_\gamma}, dE_\gamma, \quad (3.14)$$

which taking into account Eq. (3.6) allows writing the ALP yield through Primakoff scattering according to

$$\mathcal{N}_{\text{P}}^{\text{P}} = m_{\text{det}} \frac{N_T \Delta t}{4\pi L^2} \int_{E_a^{\min}}^{E_a^{\max}} \sigma_{\text{P}}^{\text{P}}(E_a) \frac{d\Phi_a^{\text{P}}}{dE_a} dE_a, \quad (3.15)$$

⁴Ref. [81] uses the two-parameter Fermi model form factor. Differences between results generated using this choice or the one we have adopted are negligible [52].

⁵We thank Bhaskar Dutta and Adrian Thompson for discussions on this subject.

⁶The inverse Primakoff differential cross section (differential cross section in detection, $d\sigma_D^{\text{P}}/dE_\gamma$) is twice as large as the one in production given in Eq. (3.8).

where $N_T = N_A/m_{\text{molar}}$ with $N_A = 6.022 \times 10^{23}/\text{mol}$ and m_{molar} the target nuclei molar mass in kg/mol (N_T thus measures the amount of nuclei/kg). Moreover, Δt stands for the data-taking time and m_{det} refers to the detector mass in kg. Integration limits are $E_a^{\text{min}} = 25 \text{ keV}$ and $E_a^{\text{max}} = 10 \text{ MeV}$ (determined by the photon natural threshold at a reactor). The second term in Eq. (3.13) is instead given by

$$\frac{d\mathcal{N}_{\text{decay}}^{\text{P}}}{dE_a} = \frac{\mathcal{A}\Delta t}{4\pi L^2} \frac{d\Phi_a^{\text{P}}}{dE_a} \mathcal{P}_{\text{decay}}, \quad (3.16)$$

where $\mathcal{P}_{\text{decay}}$ accounts for the probability that the decay occurs within the detector, and reads

$$\mathcal{P}_{\text{decay}} = 1 - e^{-L_{\text{det}}E_a/|\vec{p}_a|\tau}, \quad (3.17)$$

where L_{det} stands for the detector length and $\mathcal{A} = L_{\text{det}}^2$ denotes the detector transverse area.

3.2 Production and detection through electron-ALP coupling

The MeV photons produced in a reactor may also scatter off electrons in the materials of the reactor core and they can produce ALPs via the Compton-like process $\gamma e^- \rightarrow ae^-$. This process requires the individual SM-ALP coupling g_{aee} to be non-zero. The ALPs so produced can be subsequently detected via three possible processes relying on the same g_{aee} coupling: inverse Compton-like, axio-electric and decay into e^+e^- pairs. The total number of observed ALP events is computed similarly to the Primakoff case.

As a first step, we calculate the Compton-produced ALP flux via a convolution of the reactor photon flux $d\Phi_{\gamma'}/dE_{\gamma'}$ and the production cross section $d\sigma_{\text{P}}^{\text{C}}/dE_a$, as

$$\frac{d\Phi_a^{\text{C}}}{dE_a} = \mathcal{P}_{\text{surv}} \int_{E_{\gamma',\text{min}}}^{E_{\gamma',\text{max}}} \frac{1}{\sigma_{\text{Tot}}} \frac{d\sigma_{\text{P}}^{\text{C}}}{dE_a}(E_{\gamma'}, E_a) \frac{d\Phi_{\gamma'}}{dE_{\gamma'}} dE_{\gamma'}, \quad (3.18)$$

where we assume $E_{\gamma',\text{min}} = (2m_e m_a + m_a^2)/(2m_e)$, $E_{\gamma',\text{max}} = 10 \text{ MeV}$ and $\sigma_{\text{Tot}} = \sigma_{\text{SM}} + \sigma_{\text{P}}^{\text{C}}$. The differential Compton-like cross section for ALP production has threshold $s > (m_a + m_e)^2$ and is given by [86]

$$\frac{d\sigma_{\text{P}}^{\text{C}}}{dE_a} = \frac{Z\pi g_{aee}^2 \alpha x}{4\pi(s - m_e^2)(1 - x)E_{\gamma'}} \left[x - \frac{2m_a^2 s}{(s - m_e^2)^2} + \frac{2m_a^2}{(s - m_e^2)^2} \left(\frac{m_e^2}{1 - x} + \frac{m_a^2}{x} \right) \right], \quad (3.19)$$

where s is the Mandelstam variable and

$$x = 1 - \frac{E_a}{E_{\gamma'}} + \frac{m_a^2}{2E_{\gamma'}m_e}. \quad (3.20)$$

The total Compton-like production cross section is obtained by integrating $d\sigma_{\text{P}}/dE_a$ over the integration limits [87]:

$$x_{\text{min (max)}} = \frac{1}{2s(s - m_e^2)} [(s - m_e^2)(s - m_e^2 + m_a^2) \mp (s - m_e^2)\sqrt{(s - m_e^2 + m_a^2)^2 - 4sm_a^2}].$$

One then gets the differential number of ALP events with a second convolution, of the ALP flux $d\Phi_a/dE_a$ with the detection cross section. The latter will be different depending on the detection mechanism:

$$\frac{d\mathcal{N}_C^C}{dE_\gamma} = m_{\text{det}} \frac{N_T \Delta t}{4\pi L^2} \int_{E_{a,\text{min}}}^{E_{a,\text{max}}} \frac{d\Phi_a^C}{dE_a} \frac{d\sigma_D^C}{dE_\gamma}(E_\gamma, E_a) dE_a, \quad (3.21)$$

$$\frac{d\mathcal{N}_A^C}{dE_a} = m_{\text{det}} \frac{N_T \Delta t}{4\pi L^2} \frac{d\Phi_a^C}{dE_a} \sigma_D^A(E_\gamma, E_a), \quad (3.22)$$

$$\frac{d\mathcal{N}_{\text{decay}}^C}{dE_a} = \frac{\mathcal{A} \Delta t}{4\pi L^2} \frac{d\Phi_a^C}{dE_a} \mathcal{P}_{\text{decay}}, \quad (3.23)$$

namely inverse Compton-like, axio-electric, and e^+e^- decay, respectively. In this case, the total ALP decay width reads: $\tau^{-1} = \Gamma_{a \rightarrow e^+e^-} \times m_a/E_a$, where the $a \rightarrow e^+e^-$ decay width is

$$\Gamma_{a \rightarrow e^+e^-} = \frac{g_{aee}^2 m_a}{8\pi} \sqrt{1 - 4 \frac{m_e^2}{m_a^2}}, \quad (3.24)$$

while, the relevant detection cross sections can be cast as [88–91]

$$\begin{aligned} \frac{d\sigma_D^C}{dE_\gamma} &= \frac{Z g_{aee}^2 \alpha E_\gamma}{4m_e^2 |\vec{p}_a|} \left| \frac{2(E_a + m_e - |\vec{p}_a| \cos\theta)^2}{|\vec{p}_a| y} \right| \\ &\times \left(1 + \frac{4m_e^2 E_\gamma^2}{y^2} - \frac{4m_e E_\gamma}{y} - \frac{4m_a^2 |\vec{p}_a|^2 m_e E_\gamma (1 - \cos^2\theta)}{y^3} \right) \\ \sigma_D^A &= \frac{g_{aee}^2}{\beta} \frac{3E_a^2}{16\pi\alpha m_e^2} \left(1 - \frac{\beta^{2/3}}{3} \right) \sigma_{\text{PE}}, \end{aligned} \quad (3.25)$$

where σ_{PE} denotes the SM photoelectric cross section of the detector material. Here, θ is the scattering angle, $y = 2m_e E_a + m_a^2$ and $\beta = |\vec{p}_a|/E_a$ ⁷. The integration limits $E_{a,\text{min}} (\text{max})$ are functions of E_γ :

$$E_{a,\text{min}} = \frac{(2E_\gamma m_e - m_a^2)(E_\gamma - m_e) + E_\gamma \sqrt{(m_a^2 + 2E_\gamma m_e)^2 - 4m_a^2 m_e^2}}{2(2E_\gamma m_e - m_e^2)} \quad (3.26)$$

$$E_{a,\text{max}} = E_{\gamma',\text{max}}(1 - x_{\text{min}}) + m_a^2/(2m_e). \quad (3.27)$$

Finally, the total number of observed ALP events from Compton-like production in a reactor neutrino experiment would be

$$\begin{aligned} \mathcal{N}_C^C &= \int_{E_{\gamma,\text{min}}}^{E_{\gamma,\text{max}}} \frac{d\mathcal{N}_C^C}{dE_\gamma} dE_\gamma \\ &= m_{\text{det}} \frac{N_T \Delta t}{4\pi L^2} \int_{E_{\gamma,\text{min}}}^{E_{\gamma,\text{max}}} \int_{E_{a,\text{min}}}^{E_{a,\text{max}}} \frac{d\Phi_a^C}{dE_a} \frac{d\sigma_D^C}{dE_\gamma}(E_\gamma, E_a) dE_a dE_\gamma, \end{aligned} \quad (3.28)$$

⁷This definition of β should not be confused with the one given in Eq. (2.12).

$$\begin{aligned}
\mathcal{N}_A^C &= \int_{E_{a,1}}^{E_{a,2}} \frac{d\mathcal{N}_A^C}{dE_a} dE_a \\
&= m_{\text{det}} \frac{N_T \Delta t}{4\pi L^2} \int_{E_{a,1}}^{E_{a,2}} \frac{d\Phi_a^C}{dE_a} \sigma_D^A(E_\gamma, E_a) dE_a,
\end{aligned} \tag{3.29}$$

$$\begin{aligned}
\mathcal{N}_{\text{decay}}^C &= \int_{E_{a,1}}^{E_{a,2}} \frac{d\mathcal{N}_{\text{decay}}^C}{dE_a} dE_a \\
&= \frac{\mathcal{A} \Delta t}{4\pi L^2} \int_{E_{a,1}}^{E_{a,2}} \frac{d\Phi_a^C}{dE_a} \mathcal{P}_{\text{decay}} dE_a,
\end{aligned} \tag{3.30}$$

for the detection mechanisms inverse Compton-like, axio-electric, and e^+e^- decay, respectively. The integration limits $E_{a,1(2)}$ are extracted from the ALP flux range, whereas the final integration over E_γ is performed using the limits $E_{\gamma,\text{min}} = 25$ keV—which we assume to be the minimum detectable photon energy—and $E_{\gamma,\text{max}}$ that can be obtained by inverting Eq. (3.26), leading to the simple relation $E_{\gamma,\text{max}} = y_{\text{max}}/(2(E_{a,\text{max}} + m_e - |\vec{p}_a|))$.

3.3 Production through nucleon-ALP coupling

A heavy nucleus disintegrates through α or β decay or fission processes, while the resulting daughter nucleus is typically left in an excited state. It can then undergo fission, provided the state is above the excitation energy for this process to take place, otherwise it will in most cases decay by γ emission. The study of nuclear de-excitation follows from longitudinal (L), transverse (T), transverse-longitudinal (TL) and transverse-transverse (TT) nuclear responses. Their multipole expansion (projection in the angular momentum basis) define the Coulomb multipole operator $\widehat{M}_{JM}(q)$, the transverse electric and magnetic multipole operators $\widehat{T}_{JM}^{\text{el}}(q)$ and $\widehat{T}_{JM}^{\text{mag}}(q)$ and the longitudinal multipole operator $\widehat{L}_{JM}(q)$. The angular momentum quantum numbers J and M are determined by the angular momentum conservation conditions $|J_f - J_i| \leq J \leq J_f + J_i$ and $M = M_f - M_i$, where J_i and J_f stand for the momenta of the initial and final states involved in the nuclear excitation (or de-excitation) process (for details see e.g. [92, 93]).

For virtual photons — as e.g. those involved in electron-nucleus scattering processes — all responses matter, while for real photons only transverse electric and magnetic responses are relevant. These account for electric (magnetic) transitions EJ (MJ), with multi-polarities determined by J . The lowest orders correspond to radiation emission from charge ($J = 0$, only electric), dipole ($J = 1$) and quadrupole ($J = 2$). In addition to the angular momentum conservation, transitions are as well subject to parity conservation, for instance an EJ transition produces a photon with parity $\Pi_\gamma = (-1)^J$, while a MJ transition a photon with parity $\Pi_\gamma = (-1)^{J+1}$. Only photons for which $\Pi_\gamma = \Pi_i \Pi_f$ is satisfied are allowed. If parity is not changed, $\Delta\Pi = 0$, only even (odd) electric (magnetic) transitions are possible. If on the contrary $\Delta\Pi \neq 0$, only odd (even) electric (magnetic) transitions are available.

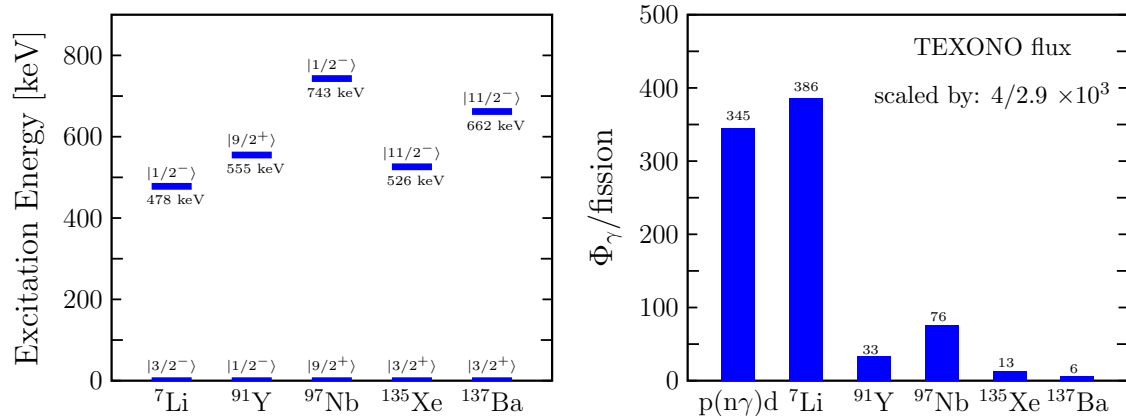


Figure 5. Left graph: $E = 478$ keV M1 transition from the excited state to the ground state of ${}^7\text{Li}$ along with M4 transitions from the excited to the ground state of ${}^{91}\text{Y}$, ${}^{97}\text{Nb}$, ${}^{135}\text{Xe}$ and ${}^{137}\text{Ba}$ (see text for more details). These transitions involve γ/a lines at 555 keV, 743 keV, 526 keV and 662 keV, respectively. **Right graph:** Photon flux for a 4 GW power plant and for each of the channels considered in our analysis. They follow from the TEXONO flux rescaled by $4/2.9$ [33].

If ALPs couple to nucleons, nuclear de-excitation can proceed as well through ALP emission. Since ALPs are pseudoscalars ($|J^\Pi\rangle = |0^-\rangle$) they can be emitted only in magnetic transitions [3], in contrast to photons which are produced in electric transitions as well. The possible quantum numbers they carry away are therefore $|0^-\rangle$, $|1^+\rangle$, $|2^-\rangle$, $|3^+\rangle$, ... [29]. To the best of our knowledge, searches for axions in magnetic transitions were pioneered by Zehnder in a nuclear decay experiment which used the 664 keV M4 transition from the $|11/2^- \rangle$ excited state to the $|3/2^+ \rangle$ ground state of ${}^{127}\text{Ba}^*$ [31]. Subsequent searches were conducted at the Bugey reactor (~ 2.8 GW) using the neutron capture M1 isovector transition along with M4 transitions in ${}^{97}\text{Nb}$, ${}^{91}\text{Y}$, ${}^{137}\text{Ba}$ and ${}^{135}\text{Xe}$ (see left graph in Fig. 5) [30]. Searches focusing on the 1115 keV M1 transition from the $|5/2^- \rangle$ excited state to the $|3/2^- \rangle$ ground state of ${}^{65}\text{Cu}$ were performed as well [32], while the same approach was later followed by Avignone et. al. [76]. More recently, similar searches were pursued at the Kuo-Sheng Nuclear Power Station by the TEXONO collaboration, which in addition to the transitions used at Bugey, considered a M1 transition in ${}^7\text{Li}$ (see left graph in Fig. 5) [33].

In our analysis we employ the fluxes reported by TEXONO: below we discuss in more detail the magnetic transitions from which they are generated. Thermal neutron capture on proton in the cooling water, $p + n \rightarrow d + \gamma$, produces a monochromatic line at 2230 keV (deuteron binding energy). The deuteron ground state has magnetic dipole and electric quadrupole moments, the emitted γ is therefore mainly M1. On the other hand, the ${}^7\text{Li}^*$ de-excitation involves M1+E2 transitions from the $|1/2^- \rangle$ first excited state to the $|3/2^- \rangle$ ground state, and so again the transition is mainly

M1. For $^{91}\text{Y}^*$ and $^{97}\text{Nb}^*$ de-excitations from the first excited state to the ground state, as shown in Fig. 5, correspond to M4 transitions. Finally, $^{135}\text{Xe}^*$ and $^{137}\text{Ba}^*$ de-excitations involve M4 transitions from the second excited state to the ground state. Note that for ^{135}Xe , de-excitation from the $|1/2^+\rangle$ first excited state to the ground state corresponds to M1+E2 transitions. If it was available, the flux from this transition (mainly M1) would be much larger than that from the M4 transition. The corresponding fluxes are shown in the right graph of Fig. 5.

ALP production depends on the ALP-nucleon couplings and on the ALP mass, while the relevant ALP flux is determined through the competition of the axion-to-photon emission rates, as first calculated in [29]. In contrast to M4 transitions, neutron capture isovector M1 transitions ($\text{pn} \rightarrow \text{d}\gamma$) depend only on kinematics and the vector ALP-nucleon coupling [94]

$$\left(\frac{\Gamma_a}{\Gamma_\gamma}\right)_{\text{pn}} = \frac{1}{2\pi\alpha} \left(\frac{|\vec{p}_a|}{|\vec{p}_\gamma|}\right)^3 \left(\frac{g_{ann}^{(1)}}{\mu_1}\right)^2, \quad (3.31)$$

where μ_1 refers to the isovector magnetic moment which follows from the neutron and proton magnetic moments, $\mu_1 = \mu_p - \mu_n = 4.71$ in nuclear magneton units $\mu_N = 1/2m_p$ (m_p is the proton mass) [76]. For MJ transitions this ratio instead involves nuclear physics input, and in the long-wavelength limit it reads [33]

$$\left(\frac{\Gamma_a}{\Gamma_\gamma}\right)_{MJ} = \frac{1}{\pi\alpha} \left(\frac{1}{1+\delta^2}\right) \left(\frac{J}{J+1}\right) \left(\frac{|\vec{p}_a|}{|\vec{p}_\gamma|}\right)^{2J+1} \left(\frac{g_{ann}^{(0)}\kappa + g_{ann}^{(1)}}{(\mu_0 - 1/2)\kappa + (\mu_1 + \eta)}\right)^2. \quad (3.32)$$

Here, μ_0 refers to the isosinglet magnetic moment normalized to μ_N and obtained as $\mu_0 = \mu_p + \mu_n = 0.88$ [76]. The remaining δ , η and κ parameters are nuclear-structure dependent. In particular, the multipole mixing ratio δ is determined by the EJ' -to- MJ ($J' = J + 1$) transition probabilities ratio, while κ and η are defined by ratios of the orbital (\hat{L}) and spin ($\hat{\sigma}$) nuclear operators reduced matrix elements, namely [76]

$$\eta = -\frac{\langle J_f || \sum_{k=1}^A \hat{L}(k) \tau_3(k) || J_i \rangle}{\langle J_f || \sum_{k=1}^A \hat{\sigma}(k) \tau_3(k) || J_i \rangle}, \quad \kappa = \frac{\langle J_f || \sum_{k=1}^A \hat{\sigma}(k) || J_i \rangle}{\langle J_f || \sum_{k=1}^A \hat{\sigma}(k) \tau_3(k) || J_i \rangle}, \quad (3.33)$$

where $J_{i,f}$ refer to initial and final state angular momenta and the sum runs over the total number of nucleons.

Values of δ , η and κ for the $^7\text{Li}^*$ M1 transition have been calculated in Refs. [95] and also adopted by the TEXONO collaboration in their analysis in [33]. The transition is an admixture of M1+E2, for which the transition probability ratio is small $\delta \ll 1$ and therefore it can be neglected, while the estimated values for η and κ are 0.5 and 1.0. For the remaining transitions $\delta = 0$, as expected since they are purely magnetic, while values for η and κ are not available. However, using results for ^{65}Cu , ^{57}Fe , ^{55}Mn and ^{23}Na —calculated in Refs. [76, 96]—TEXONO estimated these values

to be $\eta = 1$ and $\kappa = -3$ for ^{91}Y and ^{97}Nb and $\eta = -1$ and $\kappa = 1$ for ^{135}Xe and ^{137}Ba [33]. We adopt these values in our analysis.

With the values of the nuclear-structure-dependent parameters specified, we can now write the ALP flux for the i -th transition

$$\left(\frac{d\Phi_a^{\text{MT}}}{dE_a}\right)_i = \phi_a^i \delta(E_{\gamma'} - E_a) = R_f \Phi_\gamma^i \left(\frac{\Gamma_a}{\Gamma_\gamma}\right)_i \mathcal{P}_{\text{surv}} \delta(E_{\gamma'} - E_a) \quad (i = \text{p(n, } \gamma)\text{d, MJ}), \quad (3.34)$$

with Φ_γ^i the photon flux per fission for the i -th transition specified in the right graph in Fig. 5 and R_f the fission rate, which we assume that proceeds entirely from ^{235}U and estimate to be 1.248×10^{20} fissions/s for a 4 GW nuclear reactor. The ALP yield at the detector depends on the detection mechanism (see Tab. 2). In the presence of only $g_{ann}^{(a)}$ couplings, the detection would be possible only through ALP nuclear excitation. This will require the detector to be built from one of the daughter isotopes from which the ALP was produced, to enable ALP absorption. Since this does not seem to be a viable possibility, in this case we abandon our minimal assumption analysis and instead we rely on detection through Primakoff, Compton-like, axio-electric processes and decays. The nuclear de-excitation analysis is therefore sensitive to coupling pairs and the ALP mass, in contrast to the Primakoff and Compton-like analyses which determine sensitivities on a single coupling and the ALP mass.

The ALP detection rate for the i -th transition proceeds as always from a convolution of the ALP flux and the differential cross section of the corresponding detection process. For detection through inverse Primakoff, Eq. (3.14) applies and so we write

$$\left(\frac{d\mathcal{N}_P^{\text{MT}}}{dE_a}\right)_i = m_{\text{det}} \frac{N_T \Delta t}{4\pi L^2} \int \left(\frac{d\Phi_a^{\text{MT}}}{dE_a}\right)_i \frac{d\sigma_D^{\text{P}}}{dE_\gamma} dE_\gamma. \quad (3.35)$$

Using the ALP flux in Eq. (3.34) the ALP yield then becomes

$$(\mathcal{N}_P^{\text{MT}})_i = m_{\text{det}} \frac{N_T \Delta t}{4\pi L^2} \phi_a^i \sigma_D^{\text{P}}. \quad (3.36)$$

The same applies as well for detection through inverse Compton-like and axio-electric processes, for which we then write

$$(\mathcal{N}_C^{\text{MT}})_i = m_{\text{det}} \frac{N_T \Delta t}{4\pi L^2} \phi_a^i \sigma_D^{\text{C}}, \quad (\mathcal{N}_A^{\text{MT}})_i = m_{\text{det}} \frac{N_T \Delta t}{4\pi L^2} \phi_a^i \sigma_D^{\text{A}}, \quad (3.37)$$

and to ALPs detected through their decays into diphoton or electron-positron pairs:

$$(\mathcal{N}_{\text{decay}}^{\text{MT}})_i = \frac{\mathcal{A} \Delta t}{4\pi L^2} \phi_a^i \mathcal{P}_{\text{decay}}. \quad (3.38)$$

P[GW]	PM	TM	$m_{\text{det}}[\text{kg}]$	$L[\text{m}]$	$L_{\text{det}}[\text{cm}]$	bkg [1/keV/day/kg]
4	^{235}U	Ge	10	10	50	10-100
8	^{235}U	Xe	10^3	10	140	1-10

Table 4. Production and detection parameters used in our analysis. Upper values refer to current (or near-future) experiments, while those in the lower row to a next-generation experiment. These values—used for definitiveness—should be understood as representative of the actual experimental parameters shown in Tabs. 1 and 3. **P** refers to power, **PM** to production material and **TM** to target material. Our analysis includes two background hypotheses and we assume the detector to be 100% efficient.

4 Experimental sensitivities

In this section we discuss sensitivities that the experiments listed in Tab. 1 and 3 could in principle achieve. Rather than focusing on a particular case we adopt a generic analysis whose results we believe provide a general picture. To do so we fix the relevant experimental production and detection parameters as shown in Tab. 4. Upper row values provide sensitivities for ongoing or near-future experiments, while lower row values represent what could be achieved in a next-generation experiment. Given an ALP coupling, our analysis includes the processes shown in Tab. 2, the exception being the case of ALP production through nuclear de-excitations for the reasons we have discussed in Sec. 3.3. Calculation of sensitivities is done with the aid of the following χ^2 parameter function

$$\chi^2 = \frac{\mathcal{N}_{\text{ALP}}^2}{\mathcal{N}_{\text{ALP}} + \mathcal{N}_{\text{bkg}}}. \quad (4.1)$$

Here by \mathcal{N}_{ALP} we generically refer to the ALP event yield, obtained through any of the processes that we have discussed in Sec. 3, while \mathcal{N}_{bkg} refers to the background hypothesis adopted (see Tab. 4).

We begin our analysis by comparing the size of the ALP flux generated by Primakoff and Compton-like scattering as well as by M1 transitions (neutron capture in proton and $^7\text{Li}^*$ de-excitation). Figure 6 shows the result for parameter choices as displayed in the plot. One can see that a large amount of ALPs can be produced through any of the mechanisms we consider. Despite being parameter dependent, the size of the flux can become large in certain regions of the parameter space, as shown in Fig. 6. Indeed, reactor-based neutrino experiments have the potential of reaching large sensitivities, further motivating our present study. Note that M4 transitions produce a rather comparable flux to that from M1 de-excitation processes. However we found that their event yield is small (see Fig. 9), and so in the ALP-nucleon coupling analysis we consider only $p(n, d)\gamma$.

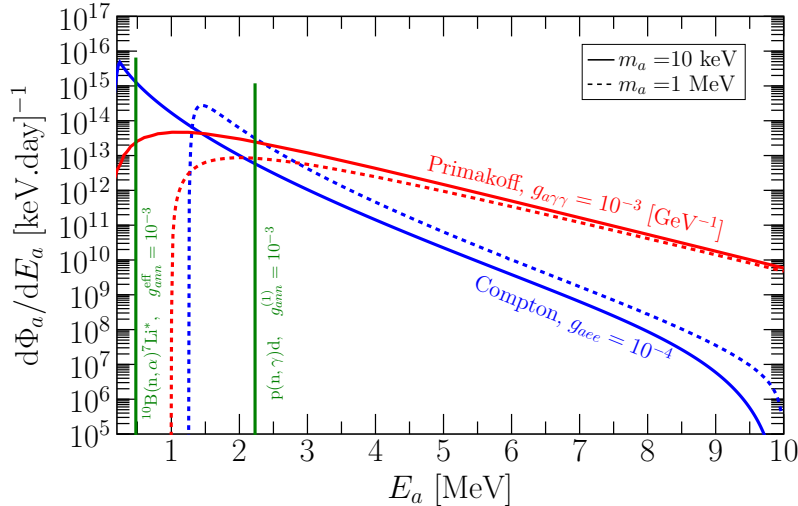


Figure 6. Typical ALP flux generated in a 4 GW nuclear power plant through Primakoff and Compton-like scattering processes as well as through neutron capture in proton and ${}^7\text{Li}^*$ de-excitation (nuclear dominant M1 transition processes). Here we have assumed $L = 10\text{ m}$ (reactor-detector distance), which is the value that we have used for the calculation of sensitivities in both current and future scenarios.

With large ALP fluxes, a large ALP event yield crucially depends on whether they can reach and decay within the detector – which is accounted for by the probabilities in Eq. (3.4). While a number of ALPs can as well interact with the detector shielding thus diminishing the expected ALP flux, for the sake of simplicity we neglect those interactions and we assume the interaction probability to be suppressed ($\mathcal{P}_{\text{det}} \rightarrow 0$). In order to demonstrate the importance of the different detector variables, we have calculated differential event rates for the Primakoff and decay $a \rightarrow \gamma\gamma$ cases (representative of models with dominant $g_{a\gamma\gamma}$ coupling⁸) varying the reactor-detector distance L , the detector mass m_{det} and the detector length L_{det} . Results are shown in Fig. 7.

One can see that the reactor-detector distance plays an important role regardless of the process, as expected given the quadratic flux dependence on that variable. Moving from 10 m to 2 m enhances the event rate by a factor 25, due to the usual isotropic reduction factor $1/(4\pi L^2)$. For $a + N \rightarrow \gamma + N$ scattering, the detector mass plays an important role as well although its effect is less pronounced than the reactor-detector distance. For $a \rightarrow \gamma\gamma$ decay the detector length is instead a key variable. As shown in the right graph in Fig. 7 a factor 5 increase in L_{det} has a

⁸A tree level $g_{a\gamma\gamma}$ coupling generates through one-loop vertex diagrams $g_{aee}^{1\text{-loop}}$ and $g_{app}^{1\text{-loop}}$ couplings. These couplings being controlled by $g_{a\gamma\gamma}$ are at least suppressed by the $1/(16\pi^2)$ loop suppression factor. The same argument applies for models with tree level g_{aee} and g_{ann} couplings. The other ALP couplings will arise at the radiative level, and so their possible effects will be suppressed.

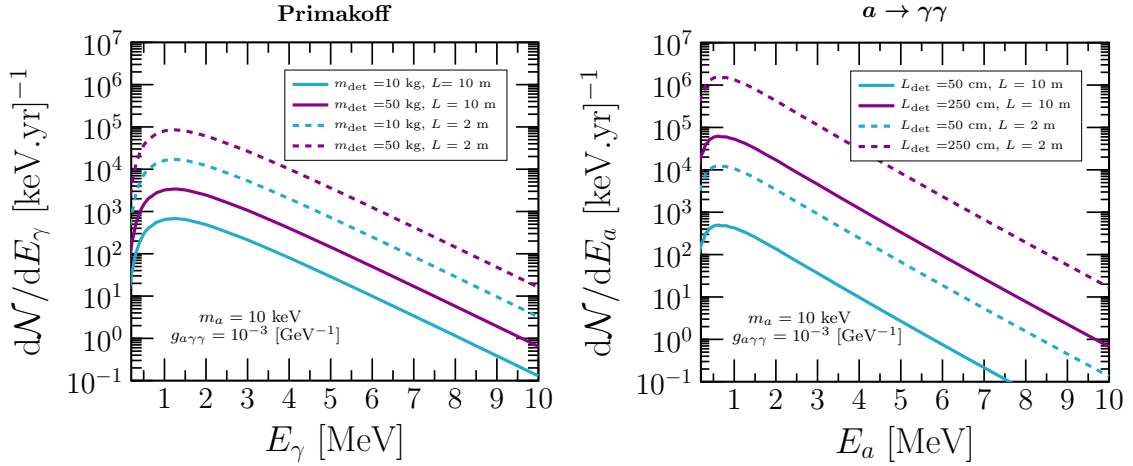


Figure 7. Left graph: ALP differential event rate for the case of production and detection through Primakoff scattering (applicable to ALP models with dominant coupling only to photons) for different values of the reactor-detector baseline and detector masses. **Right graph:** Same as in left graph, but for detection through ALP decay, $a \rightarrow \gamma\gamma$. The reactor-detector baseline as well as the detector length L_{det} vary in this case.

large impact in the event rate, resulting in an enhancement of about two orders of magnitude. From these results one can fairly conclude that, if backgrounds are well understood and under control, ideally a short reactor-detector distance combined with a large detector mass and length would maximize the ALP event rate.

As we have already stressed, for scenarios with dominant g_{aee} coupling three possible detection mechanisms are possible: Compton-like scattering, axio-electric absorption and ALP decay to electron-positron pairs. To compare their relative importance we have calculated their differential event rates for particular parameter choices. Results are shown in Fig. 8 plotted versus the relevant kinematic variable in each case. Compton-like and axio-electric absorption have about the same energy behavior, although in the former case the relevant variable is the photon energy while in the latter is the electron recoil energy. As it will become clear when discussing g_{aee} and $g_{aee} \times g_{\text{ann}}^{(1)}$ sensitivities, due to their close energy behavior they contribute similarly to the event yield. A comparison of these processes with ALP decay to electron-positron pairs shows that at large energies and for large ALP masses the decay dominates over the absorption and scattering processes. Inverse Primakoff compared with Compton-like scattering extends all over the photon energy range, but produces less events. This results in ALP-electron sensitivities being slightly better. The same applies for decays.

For scenarios with dominant g_{ann} coupling the event yield depends on the detection mechanism. For illustration, we have calculated for particular parameter space point values the different yields. Results are displayed in Fig. 9. First of all one can see the difference between M1 and M4 transitions. In all cases the event yields from

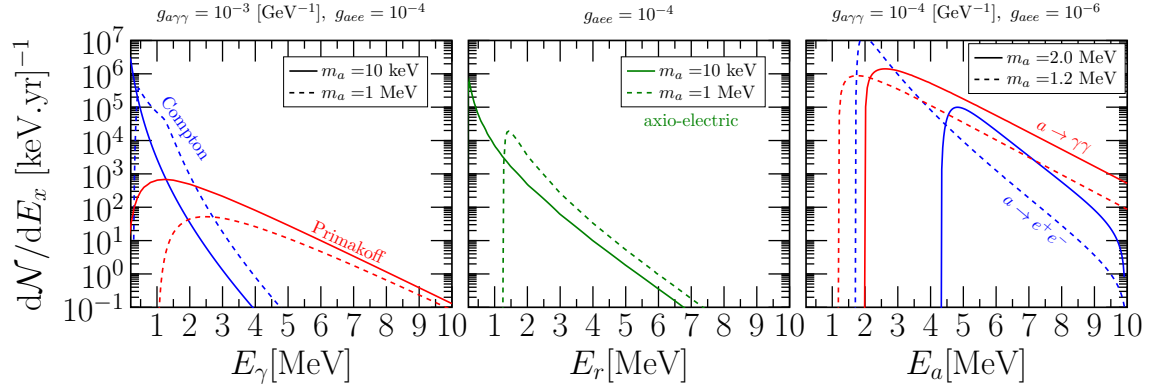


Figure 8. Differential event rate for Compton-like and Primakoff scattering (left graph), axio-electric absorption (middle graph) and ALP decay to electron-positron and photon pairs (right graph).

neutron capture in proton and ${}^7\text{Li}^*$ de-excitation exceeds that from ${}^{91}\text{Y}^*$ by more than one order of magnitude, a trend that applies for the other M4 transitions as well.

Although the ALP event rate from decay to final state photons has no kinematic constraint, its size does depend on the ALP mass as expected from Eq. (3.5). The absence of a kinematic limit allows all transitions to generate such a process, with a monochromatic event yield characterized by the energy of the corresponding transition. Decay to electron-positron pairs is instead subject to the kinematic constraint $m_a > 2m_e$, and so only $p(n, \gamma)d$ can induce such process. Although involving different numerical values, comparison of the left upper graph with the lower left graph in Fig. 9 allows to see that $a \rightarrow \gamma\gamma$ can play an important role, actually dominant once $m_a \gtrsim 10^4$ eV (this will become apparent when discussing $g_{a\gamma\gamma}$ experimental sensitivities). Comparison of the right upper graph and the middle and right lower graphs enables establishing the same conclusion, decay to electron pair dominates as soon as the channel is kinematically open. Comparison of the middle and right lower graphs in turn demonstrates that Compton-like scattering plays a more important role than axio-electric absorption does, with the event rate exceeding about an order of magnitude.

We now turn to sensitivities that could be achieved in models with dominant $g_{a\gamma\gamma}$ coupling. With the production and detection specifications we have assumed, the region of interest that can be explored corresponds to $g_{a\gamma\gamma} \gtrsim 10^{-6} \text{ GeV}^{-1}$ and $m_a \in [1, 10^7] \text{ eV}$. In this region there are various laboratory as well as astrophysical and cosmological constraints that apply. Relevant laboratory limits in the “high” mass region follow from beam-dump experiments, invisible Υ decays and $e^+e^- \rightarrow \text{inv} + \gamma$ searches [10, 11, 13–15, 97]. In the “low” mass region instead limits from CAST and SUMICO are the most important [98, 99]. Laboratory limits shown in Fig. 10 are

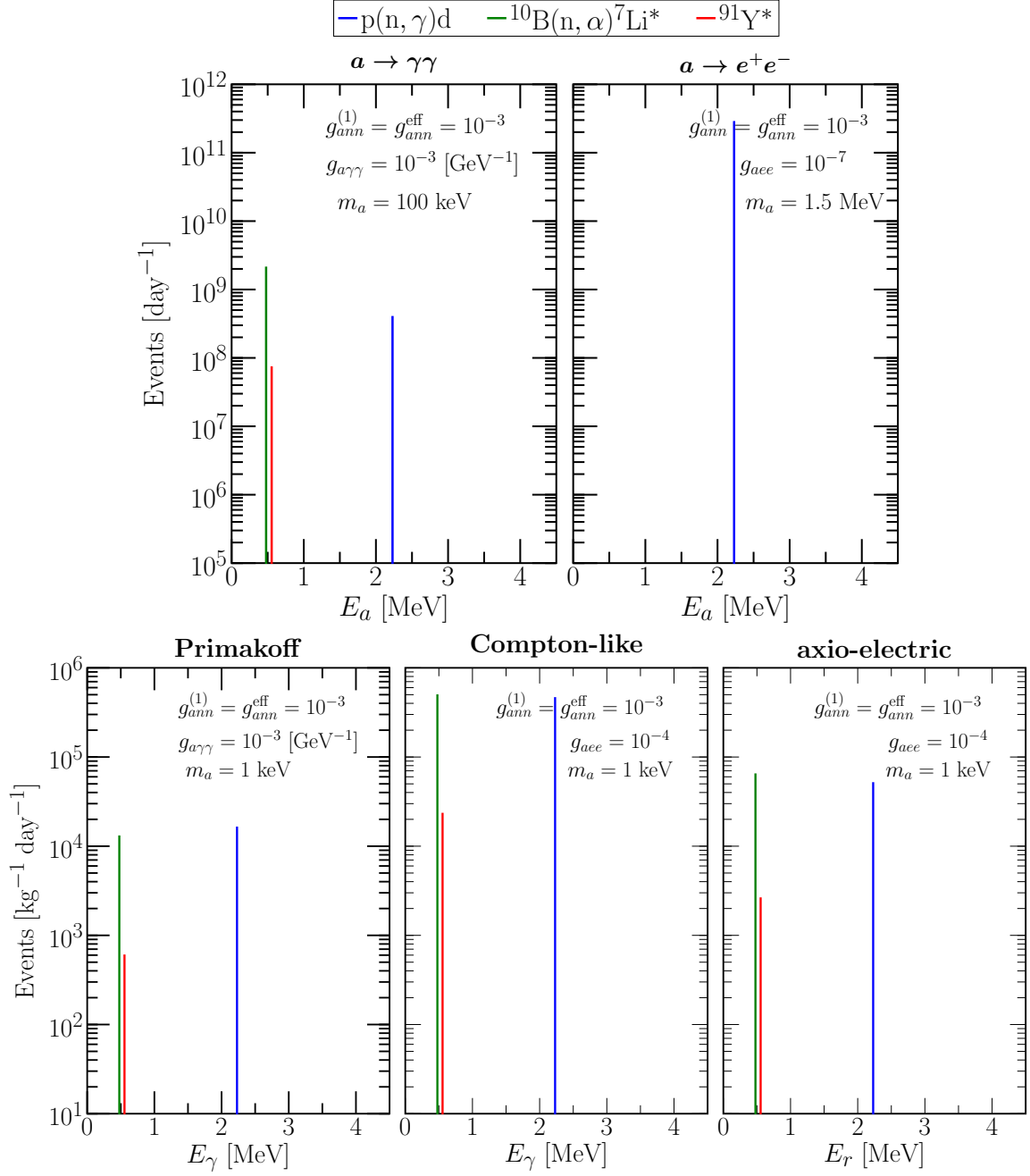


Figure 9. Event yields for ALP production through magnetic transitions and detection through: decays $a \rightarrow \gamma\gamma$ and $a \rightarrow e^+e^-$ (left and right upper graphs), inverse-Primakoff scattering $a+N \rightarrow \gamma+N$ (left lower graph), Compton-like scattering $a+e \rightarrow \gamma+e$ (middle lower graph) and axio-electric absorption $a+e+Z \rightarrow \gamma+e+Z$ (right lower graph). The event yield has been calculated for a 4 GW reactor power plant assuming $L = 10$ m. Here, $g_{ann}^{eff} = g_{ann}^{(0)}\kappa + g_{ann}^{(1)}$.

adapted from Ref. [100]. Although our analysis applies for ALPs, for completeness we show the region of hadronic QCD axion models defined by $E/N \subset [5/3, 44/3]$ [65].

Constraints from astrophysical sources are derived from SN1987A and horizontal branch (HB) stars [101–106]. SN1987A limits follow from SN energy loss, which in the absence of ALPs is driven by neutrino emission, and from the visible signal that ALP emission and subsequent decay to photons will generate. Given the temperature of the SN environment, these bounds extend up to ALP masses of the order of 10^8 eV. Horizontal branch stars limits follow, instead, from stellar cooling arguments. The presence of the new coupling opens a channel that accelerates the consumption of helium resulting in a reduction of the HB stars lifetime [107]. It is worth emphasizing that the SN limit is subject to large uncertainties, mainly due to the lack of a detailed understanding of the SN1987A. Actually it has been recently pointed out that it might not apply at all [108]. HB stars bounds as well as CAST+SUMICO [98, 109–111] limits can be substantially relaxed if the photon-ALP coupling and ALP mass depend on environmental conditions such as the matter density and temperature, see e.g. [112] and references therein.

The triangular white region in Fig. 10, the so-called *cosmological triangle*, is subject as well to cosmological constraints of which BBN and N_{eff} are particularly relevant [113–115]. Under standard cosmological arguments (Λ CDM) with a high inflationary scale that region is therefore ruled out. Departures from standard arguments, however, open this spot in parameter space. Possible scenarios include low-reheating temperature (T_R) models, extra contributions to the radiation energy density and non-vanishing neutrino chemical potentials [114, 115]. Let us take the case of low-reheating models. If $T_R \gg T_{\text{fo}}$, where T_{fo} is the Primakoff freeze-out temperature, ALPs are abundant in the heat bath. Photons produced by the decay of this thermal ALP distribution will then dilute the baryon density and disrupt N_{eff} , the former affecting BBN. If instead $T_R \ll T_{\text{fo}}$ —and ALPs are not produced by e.g. inflaton decays—ALPs will be much less abundant and so the amount of photons injected in the heat bath [115], thus having a small effect on BBN and N_{eff} .

From Fig. 10 one can see that 90%CL sensitivities will cover regions where CAST and SUMICO as well as the SN 1987A and HB stars cooling arguments have placed limits. As we have mentioned, these bounds can be evaded if environmental effects—relevant in stellar interiors—are at work. Reactor experiment measurements therefore will be able to test whether such effects are present. Sensitivities cover as well the cosmological triangle, thus implying that this type of measurements will test the cosmological hypotheses behind the constraints in that region. These searches therefore will be complementary to those that will be carried out at BELLE-II (50 ab^{-1}) [116]. Undergoing and near-future experiments will partially cover that region and next-generation experiments will complement those measurements, allowing to cover the full region .

In models with dominant g_{aee} coupling there are as well limits in the region that

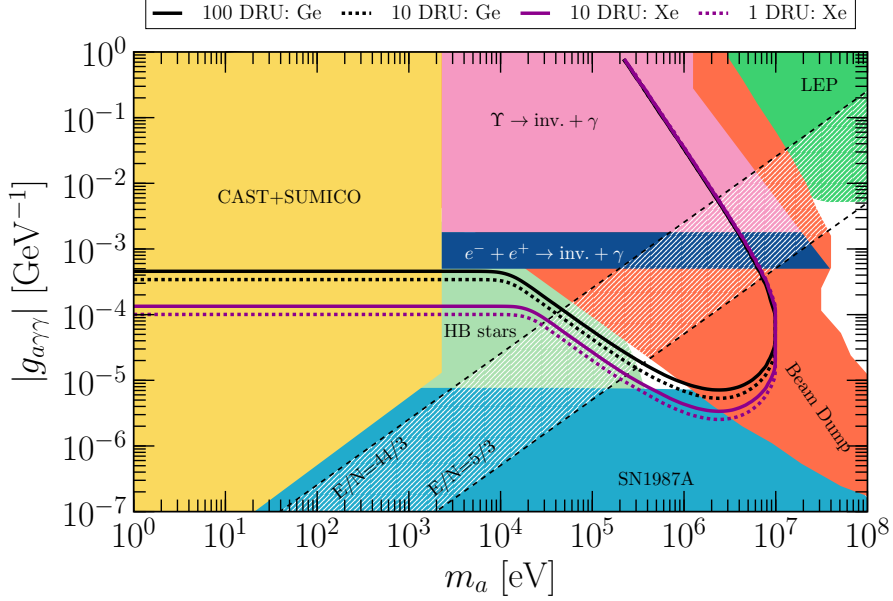


Figure 10. Photon-ALP coupling 90%CL sensitivities along with relevant laboratory, astrophysical and cosmological limits that apply in the region of interest, adapted from Ref. [100, 105, 106]. Black contours correspond to 90%CL sensitivities achievable with ongoing or near-future experiments (see Tab. 3). Purple contours instead indicate 90%CL sensitivities that could be achieved in a next generation experiment. Solid (dotted) contours refer to sensitivities under the assumption of a background rate of 100 DRU (10 DRU) for ongoing or near-future experiments, while to 10 DRU (1 DRU) for a next generation setup. See the text for more details. For completeness we show as well the region covered by QCD axion models, with QCD and electromagnetic anomaly coefficients fixed according to Ref. [65].

reactor experiments can cover, $g_{aee} \gtrsim 10^{-8}$ and in the same ALP mass range as that of the $g_{a\gamma\gamma}$ case. In the “low” mass window Red Giants cooling arguments as well as ALP searches at the EDELWEISS III experiment place the most relevant bounds [117, 118]. At “high” ALP masses beam dump experiments are important [119]. These limits along with the sensitivities that could be achieved in current, near-future or next generation experiments are displayed in Fig. 11. We show as well the region covered by the DFSZ-I and DFSZ-II QCD axion models.

From Fig. 11 one can see that the region $m_a \in [5, 20] \times 10^5$ eV is not subject to constraints. Inverse Compton-like scattering and axio-electric absorption will allow testing couplings down to $\sim 10^{-5}$ in that region, with the precise value determined by how well backgrounds are kept under control. Smaller values might be achievable in next generation experiments. Decay to electron-positron pairs extends the region that can be covered in that mass window, extending sensitivities down to couplings of order $g_{aee} \sim 10^{-8}$. Inverse Compton-like scattering and axio-electric absorption cover as well regions subject to limits from Red Giants cooling arguments and EDELWEISS

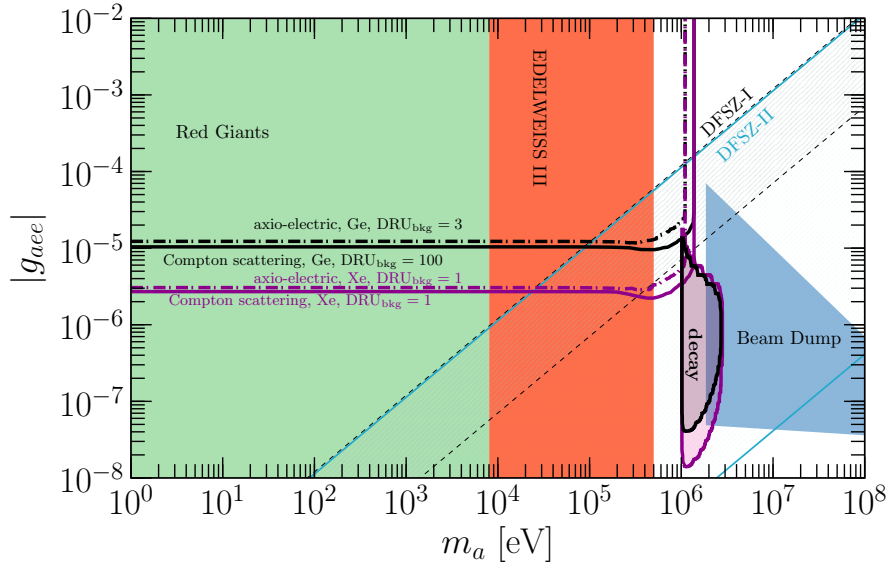


Figure 11. Electron-ALP coupling 90%CL sensitivities along with relevant laboratory and astrophysical limits that apply in the region of interest. Black contours correspond to 90%CL sensitivities achievable with ongoing or near-future experiments (see Tab. 2). Purple contours instead indicate 90%CL sensitivities that could be achieved in a next-generation xenon detector. Solid (dashed-dotted) contours refer to sensitivities under the assumption of detection via inverse Compton-like scattering (axio-electric absorption) and different background rates. See the text for more details. For completeness we show as well the region of DFSZ-I and DFSZ-II QCD axion models.

III. Since the latter searches for solar ALPs, sensitivities in the region $m_a \lesssim 5 \times 10^5$ eV will test as well possible scenarios (hypotheses) where environmental effects could allow circumventing those limits.

Finally our results for ALP models with dominant (tree level) $g_{ann}^{(1)}$ and $g_{a\gamma\gamma}$ couplings ($g_{ann}^{(1)}$ and g_{aee} couplings) are shown in the left graph (right graph) in Fig. 12⁹. Relevant constraints follow from TEXONO [33], Borexino [120, 121] and BGO [122, 123], that cover ALP mass values up to 10^6 eV. Constraints from solar ALP searches using ^{57}Fe first excited state and detection through axio-electric absorption apply in the case of the $g_{aee} \times g_{ann}^{(1)}$ combination. Those limits follow from a variety of experiments, namely EDELWEISS III [118], PANDAX-II [124], CDEX [125] and the MAJORANA DEMONSTRATOR [126]. Due to kinematic constraints they cover the ALP mass range $[1, 14.4 \times 10^3]$ eV. In the case of the $g_{a\gamma\gamma} \times g_{ann}^{(1)}$ combination we include HB stars cooling and SN1987A energy loss limits, which should be interpreted as subject to the constraints the individual couplings

⁹Due to the survival and decay probabilities the ALP yield has a non-trivial dependence on the ALP couplings. This is accounted for in our statistical analysis by varying the two couplings and the ALP mass independently. So although the plotting is done by using the product of couplings as the relevant variable, the results include the non-trivial coupling dependence.

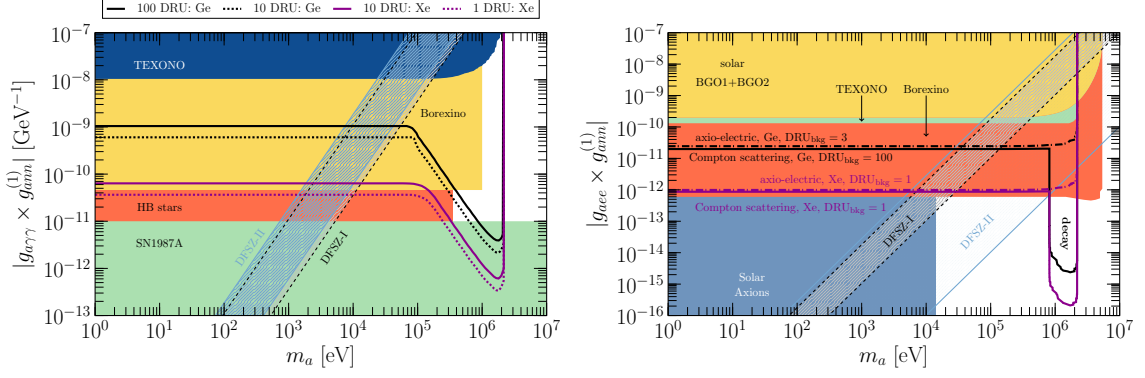


Figure 12. Left graph: Photon-ALP times nucleon-ALP couplings 90%CL sensitivities along with relevant laboratory and astrophysical limits in the region of interest. Black contours correspond to 90%CL sensitivities achievable with ongoing or near-future experiments (see Tab. 3). Purple contours instead indicate 90%CL sensitivities that could be achieved in a next-generation xenon detector. Solid (dotted) contours refer to sensitivities under the assumption different background rates, (see the legend). **Right graph:** Same as in left graph but for electron-ALP times nucleon-ALP couplings sensitivities. Here solid (dot-dashed) curves correspond to detection via inverse Compton-like scattering and decays into electron-positron pairs (axio-electric absorption), with different background rates. The solar axion region includes limits from EDELWEISS III, MAJORANA DEMONSTRATOR, CDEX and PandaX-II [118, 124–126]. For completeness we include the region of DFSZ-I and DFSZ-II QCD axion models.

are subject to, $g_{a\gamma\gamma} \lesssim 2 \times 10^{-6} \text{ GeV}^{-1}$ (see Fig. 10) and $g_{ann}^{(1)} \lesssim 5 \times 10^{-6}$ [127]. As we have done in the previous cases, we include as well the region covered by the DFSZ-I and DFSZ-II QCD axion models.

In the case of detection through inverse Primakoff and ALP decay to photons, 90%CL sensitivity contours in the low mass range include regions covered by TEXONO and Borexino searches. For ALP masses above $\sim 4 \times 10^5 \text{ eV}$ and up to kinematic threshold $\sim 2 \times 10^6 \text{ eV}$, ALP decay will widen searches in parameter space. Furthermore 90%CL sensitivities go inside some of the HB stars and SN1987A regions. These measurements therefore can partially—and potentially—test the hypotheses behind these constraints. Detection through g_{aee} -related processes also cover Borexino and TEXONO regions, but more importantly will access an ALP mass stripe within $[8, 20] \times 10^5 \text{ eV}$ and down to couplings of order 10^{-15} . We have also shown that next-generation experiments have the capability to substantially improve those sensitivities.

There is an infinite set of individual couplings g_{aXX} ($X = \gamma, e$) and $g_{ann}^{(1)}$ that satisfy the condition $g_{aXX} \times g_{ann}^{(1)} = \text{const}$, which is not explicit in our results in Fig. 12. The interplay of the individual couplings on sensitivities can be seen in Fig. 13, which shows the 90%CL sensitivities calculated in the two-dimensional coupling plane for

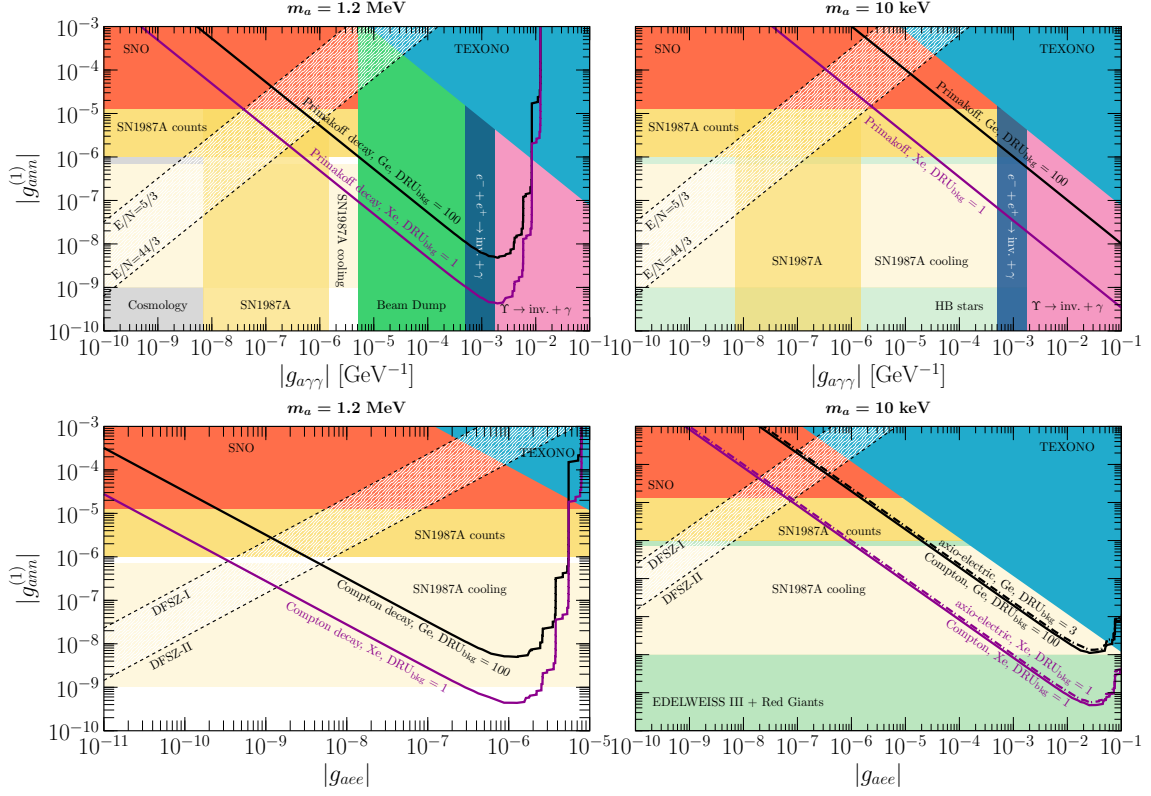


Figure 13. 90%CL sensitivities in ALP production through magnetic de-excitation and detection through $g_{a\gamma\gamma}$ and g_{aee} related processes. Results are displayed in the couplings plane for a fixed ALP mass. See text for more details. Bounds on the isovector axion-nucleon coupling $g_{ann}^{(1)}$ are adapted from [128]. For completeness we include the region of DFSZ-I and DFSZ-II QCD axion models.

fixed ALP mass along with the limits the individual couplings are subject to. For illustrative purposes, we have fixed $m_a = 1.2$ MeV (10 keV) for the left (right) graphs in Fig. 13, depicting sensitivities for ALPs detected via decay (scattering) processes, respectively. Indeed, decays are more relevant at higher masses, while scattering processes lead to almost constant number of events for masses $m_a \lesssim 10^4$ (10^5) eV for Primakoff (Compton-like, axio-electric) detection mechanisms. From these plots one can see that most of the parameter space inside these sensitivities is already probed by a variety of different experiments, from laboratory to astrophysics and cosmology [128, 129]. In the case of decays however, reactor searches could probe some small regions of parameter space currently uncovered, at $g_{ann}^{(1)} \lesssim 10^{-9}$ and $g_{aee} \sim 10^{-6}$, or in the “cosmological triangle” region at $g_{ann}^{(1)} \sim 10^{-6}$ and $g_{a\gamma\gamma} \sim 5 \times 10^{-6}$. In the rest of parameter space, reactor searches would still give valuable information, by providing complementary laboratory probes especially in the regions currently tested only by astrophysical observations.

5 Conclusions

Nuclear reactor power plants produce a large amount of photons and so they are suitable sources for ALPs production. In this paper we have studied such possibility by considering production through three possible mechanisms: Compton-like and Primakoff scattering as well as nuclear de-excitation in the fuel material. Motivated by the current CE ν NS experimental program, which aims at observing CE ν NS induced by reactor neutrino fluxes using various low-threshold technologies, we have analyzed the prospects for detection of ALPs in such experiments. We have assumed a 10 kg germanium detector, which we regard as representative of current (CONUS [36]) or near-future CE ν NS experiments (including MINER [35], Ricochet [38], ν GeN [70] and TEXONO [40]). We have also explored future capabilities of next generation experiments, assuming a ton-scale xenon detector.

Concerning ALPs detection, we have considered processes controlled by the same couplings that determine their production. Namely, we have focused on inverse-Primakoff scattering and ALP decays into photons for production through Primakoff scattering (processes controlled by $g_{a\gamma\gamma}$), while we have investigated inverse Compton-like scattering, axio-electric absorption and decay into electron pairs for ALPs produced through Compton-like scattering (processes controlled by g_{aee}). For nuclear de-excitation we have instead considered detection through processes controlled by $g_{a\gamma\gamma}$ and g_{aee} couplings.

We have calculated 90%CL sensitivities to ALPs in the mass range ($1 - 10^7$ eV), and we have confronted them to existing constraints. Our main results are displayed in Figs. 10-13, and they can be summarized as follows. For models with dominant $g_{a\gamma\gamma}$ coupling, these experiments will probe a region in the ALP mass range around 1 MeV, presently constrained only by cosmological observations. Moreover, since reactor searches will cover regions currently constrained by CAST+SUMICO, SN 1987A and HB stars cooling arguments, they can also potentially test ALPs environment-dependent properties in stellar media. For ALP models with dominant ALP-electron coupling, reactor searches will probe ALP masses in the range $[5, 20] \times 10^5$ eV and ALP-electron couplings extending down to $g_{aee} \sim 10^{-8}$. They will also cover regions constrained by Red Giants cooling arguments as well as by EDELWEISS III solar axions searches, thus testing also in this case the potential relevance of ALP environmental effects.

Searches for ALPs produced in nuclear de-excitation require the presence of two different ALP-SM couplings. If detection proceeds through ALP-photon coupling induced-processes, they can improve current limits set by Borexino solar axion searches and by the TEXONO reactor experiment in the ALP mass range $\sim [0.2, 2]$ MeV. Moreover these searches could probe regions constrained by SN1987A data and so the different hypotheses this limit comes along with. Detection through ALP-electron coupling induced-processes will cover regions already explored by other

experiments such as BGO, Borexino and TEXONO. Still, a small region in parameter space (currently unexplored) with ALP masses \sim MeV and couplings $g_{ann}^{(1)} \sim 10^{-9}$ could be tested.

To summarize, we have considered the possibility that ongoing and near-future reactor-based CE ν NS experiments can be used for ALP searches. Of course these searches could be run in any other reactor-based experiment. However since CE ν NS experiments will run anyway, they will probably be the most suited environment for these type of searches. We have shown that sensitivities can cover interesting regions in the ALP parameter space not yet explored by laboratory experiments, thus motivating the inclusion of ALP searches in the physics program of such reactor neutrino experiments.

Acknowledgment

We thank Bhaskar Dutta and Adrian Thompson for very useful discussions and providing us details of their calculation in Ref. [55]. We thank Henry Wong for useful comments and Enrico Nardi for comments on the manuscript. We are also very grateful to Alessandro Mirizzi for pointing out useful updates of the astrophysical bounds from Globular Cluster stars and SN 1987A. DAS is supported by the grant ‘‘Unraveling new physics in the high-intensity and high-energy frontiers’’, Fondecyt No. 1171136. VDR acknowledges financial support by the SEJI/2020/016 grant (project ‘‘Les Fosques’’), funded by Generalitat Valenciana and partial support by the Spanish grants FPA2017-90566-REDC (Red Consolider MultiDark), FPA2017-85216-P and PROMETEO/2018/165 (Generalitat Valenciana). LJF is supported by a posdoctoral CONACYT grant, CONACYT CB2017-2018/A1-S-13051 (Mexico) and DGAPA-PAPIIT IN107118/IN107621. The work of DKP is co-financed by Greece and the European Union (European Social Fund- ESF) through the Operational Programme ‘‘Human Resources Development, Education and Lifelong Learning’’ in the context of the project ‘‘Reinforcement of Postdoctoral Researchers - 2nd Cycle’’ (MIS-5033021), implemented by the State Scholarships Foundation (IKY).

References

- [1] R. Peccei and H. R. Quinn, *CP Conservation in the Presence of Instantons*, *Phys. Rev. Lett.* **38** (1977) 1440.
- [2] R. Peccei and H. R. Quinn, *Constraints Imposed by CP Conservation in the Presence of Instantons*, *Phys. Rev. D* **16** (1977) 1791.
- [3] S. Weinberg, *A New Light Boson?*, *Phys. Rev. Lett.* **40** (1978) 223.
- [4] F. Wilczek, *Problem of Strong P and T Invariance in the Presence of Instantons*, *Phys. Rev. Lett.* **40** (1978) 279.

- [5] A. Davidson and K. C. Wali, *MINIMAL FLAVOR UNIFICATION VIA MULTIGENERATIONAL PECCEI-QUINN SYMMETRY*, *Phys. Rev. Lett.* **48** (1982) 11.
- [6] F. Wilczek, *Axions and Family Symmetry Breaking*, *Phys. Rev. Lett.* **49** (1982) 1549.
- [7] Y. Chikashige, R. N. Mohapatra and R. Peccei, *Are There Real Goldstone Bosons Associated with Broken Lepton Number?*, *Phys. Lett. B* **98** (1981) 265.
- [8] I. G. Irastorza and J. Redondo, *New experimental approaches in the search for axion-like particles*, *Prog. Part. Nucl. Phys.* **102** (2018) 89 [1801.08127].
- [9] L. Di Luzio, M. Giannotti, E. Nardi and L. Visinelli, *The landscape of QCD axion models*, *Phys. Rept.* **870** (2020) 1 [2003.01100].
- [10] M. Krasny et al., *RECENT SEARCHES FOR SHORTLIVED PSEUDOSCALAR BOSONS IN ELECTRON BEAM DUMP EXPERIMENTS*, in *International Europhysics Conference on High-energy Physics*, 6, 1987.
- [11] B. Döbrich, *Axion-like Particles from Primakov production in beam-dumps*, *CERN Proc.* **1** (2018) 253 [1708.05776].
- [12] E. Riordan et al., *A Search for Short Lived Axions in an Electron Beam Dump Experiment*, *Phys. Rev. Lett.* **59** (1987) 755.
- [13] J. Bjorken, S. Ecklund, W. Nelson, A. Abashian, C. Church, B. Lu et al., *Search for Neutral Metastable Penetrating Particles Produced in the SLAC Beam Dump*, *Phys. Rev. D* **38** (1988) 3375.
- [14] CRYSTAL BALL collaboration, *Limits on axion and light Higgs boson production in Upsilon (1s) decays*, *Phys. Lett. B* **251** (1990) 204.
- [15] BABAR collaboration, *Search for Invisible Decays of a Light Scalar in Radiative Transitions $v_{3S} \rightarrow \gamma A_0$* , in *34th International Conference on High Energy Physics*, 7, 2008, 0808.0017.
- [16] OPAL collaboration, *Photonic events with missing energy in e^+e^- collisions at $\sqrt{s} = 189\text{GeV}$* , *Eur. Phys. J. C* **18** (2000) 253 [hep-ex/0005002].
- [17] ATLAS collaboration, *Evidence for light-by-light scattering in heavy-ion collisions with the ATLAS detector at the LHC*, *Nature Phys.* **13** (2017) 852 [1702.01625].
- [18] M. Bauer, M. Neubert and A. Thamm, *Collider Probes of Axion-Like Particles*, *JHEP* **12** (2017) 044 [1708.00443].
- [19] M. Bauer, M. Heiles, M. Neubert and A. Thamm, *Axion-Like Particles at Future Colliders*, *Eur. Phys. J. C* **79** (2019) 74 [1808.10323].
- [20] BELLE-II collaboration, *Belle II Technical Design Report*, 1011.0352.
- [21] NA62 collaboration, *The Beam and detector of the NA62 experiment at CERN*, *JINST* **12** (2017) P05025 [1703.08501].

- [22] S. Gardner, R. Holt and A. Tadepalli, *New Prospects in Fixed Target Searches for Dark Forces with the SeaQuest Experiment at Fermilab*, *Phys. Rev. D* **93** (2016) 115015 [[1509.00050](#)].
- [23] A. Berlin, S. Gori, P. Schuster and N. Toro, *Dark Sectors at the Fermilab SeaQuest Experiment*, *Phys. Rev. D* **98** (2018) 035011 [[1804.00661](#)].
- [24] J. P. Chou, D. Curtin and H. Lubatti, *New Detectors to Explore the Lifetime Frontier*, *Phys. Lett. B* **767** (2017) 29 [[1606.06298](#)].
- [25] D. Curtin and M. E. Peskin, *Analysis of Long Lived Particle Decays with the MATHUSLA Detector*, *Phys. Rev. D* **97** (2018) 015006 [[1705.06327](#)].
- [26] G. Aielli et al., *Expression of Interest for the CODEX-b Detector*, [1911.00481](#).
- [27] SHiP collaboration, *A facility to Search for Hidden Particles (SHiP) at the CERN SPS*, [1504.04956](#).
- [28] NA64 collaboration, *Search for Axionlike and Scalar Particles with the NA64 Experiment*, *Phys. Rev. Lett.* **125** (2020) 081801 [[2005.02710](#)].
- [29] T. Donnelly, S. Freedman, R. Lytel, R. Peccei and M. Schwartz, *Do Axions Exist?*, *Phys. Rev. D* **18** (1978) 1607.
- [30] J. Cavaignac et al., *A Search for Axions at a Power Reactor*, *Phys. Lett. B* **121** (1983) 193.
- [31] A. Zehnder, *Axion Search in a Monochromatic γ Transition: A New Lower Limit for the Axion Mass*, *Phys. Lett. B* **121** (1981) 184.
- [32] P. Lehmann, E. Lesquoy, A. Muller and S. Zylberajch, *AXION SEARCH IN THE MONOCHROMATIC M1 TRANSITION OF CU-65*, *Phys. Lett. B* **115** (1982) 270.
- [33] TEXONO collaboration, *Search of axions at the Kuo-Sheng nuclear power station with a high-purity germanium detector*, *Phys. Rev.* **D75** (2007) 052004 [[hep-ex/0609001](#)].
- [34] CONNIE collaboration, *Exploring Low-Energy Neutrino Physics with the Coherent Neutrino Nucleus Interaction Experiment (CONNIE)*, [1906.02200](#).
- [35] MINER collaboration, *Background Studies for the MINER Coherent Neutrino Scattering Reactor Experiment*, *Nucl. Instrum. Meth. A* **853** (2017) 53 [[1609.02066](#)].
- [36] J. Hakenmüller et al., *Neutron-induced background in the CONUS experiment*, *Eur. Phys. J. C* **79** (2019) 699 [[1903.09269](#)].
- [37] R. Strauss et al., *The ν -cleus experiment: A gram-scale fiducial-volume cryogenic detector for the first detection of coherent neutrino-nucleus scattering*, *Eur. Phys. J. C* **77** (2017) 506 [[1704.04320](#)].
- [38] J. Billard et al., *Coherent Neutrino Scattering with Low Temperature Bolometers at Chooz Reactor Complex*, *J. Phys. G* **44** (2017) 105101 [[1612.09035](#)].
- [39] D. Akimov et al., *Status of the RED-100 experiment*, *JINST* **12** (2017) C06018.

- [40] H. T.-K. Wong, *Taiwan EXperiment On Neutrino — History and Prospects*, *The Universe* **3** (2015) 22 [[1608.00306](#)].
- [41] D. Yu. Akimov, V. A. Belov, A. Bolozdynya, Yu. V. Efremenko, A. M. Konovalov, A. V. Kumpan et al., *Coherent elastic neutrino scattering on atomic nucleus: recently discovered type of low-energy neutrino interaction*, *Phys. Usp.* **62** (2019) 166.
- [42] O. G. Miranda, G. Sanchez Garcia and O. Sanders, *Coherent elastic neutrino-nucleus scattering as a precision test for the Standard Model and beyond: the COHERENT proposal case*, *Adv. High Energy Phys.* **2019** (2019) 3902819 [[1902.09036](#)].
- [43] C. Giunti, *General COHERENT constraints on neutrino nonstandard interactions*, *Phys. Rev. D* **101** (2020) 035039 [[1909.00466](#)].
- [44] O. G. Miranda, D. K. Papoulias, M. Tórtola and J. W. F. Valle, *Probing neutrino transition magnetic moments with coherent elastic neutrino-nucleus scattering*, *JHEP* **07** (2019) 103 [[1905.03750](#)].
- [45] M. Lindner, W. Rodejohann and X.-J. Xu, *Coherent Neutrino-Nucleus Scattering and new Neutrino Interactions*, *JHEP* **03** (2017) 097 [[1612.04150](#)].
- [46] Y. Farzan, M. Lindner, W. Rodejohann and X.-J. Xu, *Probing neutrino coupling to a light scalar with coherent neutrino scattering*, *JHEP* **05** (2018) 066 [[1802.05171](#)].
- [47] D. Aristizabal Sierra, V. De Romeri and N. Rojas, *COHERENT analysis of neutrino generalized interactions*, *Phys. Rev.* **D98** (2018) 075018 [[1806.07424](#)].
- [48] J. Liao and D. Marfatia, *COHERENT constraints on nonstandard neutrino interactions*, *Phys. Lett.* **B775** (2017) 54 [[1708.04255](#)].
- [49] D. Aristizabal Sierra, N. Rojas and M. H. G. Tytgat, *Neutrino non-standard interactions and dark matter searches with multi-ton scale detectors*, *JHEP* **03** (2018) 197 [[1712.09667](#)].
- [50] D. Aristizabal Sierra, B. Dutta, S. Liao and L. E. Strigari, *Coherent elastic neutrino-nucleus scattering in multi-ton scale dark matter experiments: Classification of vector and scalar interactions new physics signals*, *JHEP* **12** (2019) 124 [[1910.12437](#)].
- [51] D. Aristizabal Sierra, V. De Romeri and N. Rojas, *CP violating effects in coherent elastic neutrino-nucleus scattering processes*, *JHEP* **09** (2019) 069 [[1906.01156](#)].
- [52] D. Aristizabal Sierra, J. Liao and D. Marfatia, *Impact of form factor uncertainties on interpretations of coherent elastic neutrino-nucleus scattering data*, *JHEP* **06** (2019) 141 [[1902.07398](#)].
- [53] D. Papoulias, T. Kosmas and Y. Kuno, *Recent probes of standard and non-standard neutrino physics with nuclei*, *Front. in Phys.* **7** (2019) 191 [[1911.00916](#)].
- [54] L. Flores, N. Nath and E. Peinado, *Non-standard neutrino interactions in $U(1)'$ model after COHERENT data*, *JHEP* **06** (2020) 045 [[2002.12342](#)].

- [55] J. B. Dent, B. Dutta, D. Kim, S. Liao, R. Mahapatra, K. Sinha et al., *New Directions for Axion Searches via Scattering at Reactor Neutrino Experiments*, *Phys. Rev. Lett.* **124** (2020) 211804 [[1912.05733](#)].
- [56] Y. Nomura and J. Thaler, *Dark Matter through the Axion Portal*, *Phys. Rev. D* **79** (2009) 075008 [[0810.5397](#)].
- [57] B. Batell, M. Pospelov and A. Ritz, *Exploring Portals to a Hidden Sector Through Fixed Targets*, *Phys. Rev. D* **80** (2009) 095024 [[0906.5614](#)].
- [58] J. Schechter and J. Valle, *Neutrino Decay and Spontaneous Violation of Lepton Number*, *Phys. Rev. D* **25** (1982) 774.
- [59] A. Arvanitaki, S. Dimopoulos, S. Dubovsky, N. Kaloper and J. March-Russell, *String Axiverse*, *Phys. Rev. D* **81** (2010) 123530 [[0905.4720](#)].
- [60] M. Cicoli, M. Goodsell and A. Ringwald, *The type IIB string axiverse and its low-energy phenomenology*, *JHEP* **10** (2012) 146 [[1206.0819](#)].
- [61] J. E. Kim, *Weak Interaction Singlet and Strong CP Invariance*, *Phys. Rev. Lett.* **43** (1979) 103.
- [62] M. A. Shifman, A. Vainshtein and V. I. Zakharov, *Can Confinement Ensure Natural CP Invariance of Strong Interactions?*, *Nucl. Phys. B* **166** (1980) 493.
- [63] A. Zhitnitsky, *On Possible Suppression of the Axion Hadron Interactions. (In Russian)*, *Sov. J. Nucl. Phys.* **31** (1980) 260.
- [64] M. Dine, W. Fischler and M. Srednicki, *A Simple Solution to the Strong CP Problem with a Harmless Axion*, *Phys. Lett. B* **104** (1981) 199.
- [65] L. Di Luzio, F. Mescia and E. Nardi, *Redefining the Axion Window*, *Phys. Rev. Lett.* **118** (2017) 031801 [[1610.07593](#)].
- [66] M. Roos, *Sources of Gamma Radiation in a Reactor Core*, *Phys. Lett. B* **1** (1959) 98.
- [67] H. Bechteler et al., *The spectrum of γ radiation emitted in the FRJ-1 (Merlin) reactor core and moderator region*, tech. rep., Inst. fuer Kernphysik, 1984.
- [68] H. Park, *Detecting Dark Photons with Reactor Neutrino Experiments*, *Phys. Rev. Lett.* **119** (2017) 081801 [[1705.02470](#)].
- [69] S.-F. Ge and I. M. Shoemaker, *Constraining Photon Portal Dark Matter with Texono and Coherent Data*, [1710.10889](#).
- [70] V. Belov et al., *The ν GeN experiment at the Kalinin Nuclear Power Plant*, *JINST* **10** (2015) P12011.
- [71] E. Vásquez. Private communication, Sept., 2020.
- [72] G. Fernandez Moroni, J. Estrada, E. E. Paolini, G. Canelo, J. Tiffenberg and J. Molina, *Charge Coupled Devices for detection of coherent neutrino-nucleus scattering*, *Phys. Rev. D* **91** (2015) 072001 [[1405.5761](#)].

- [73] G. Fernandez-Moroni, P. A. Machado, I. Martinez-Soler, Y. F. Perez-Gonzalez, D. Rodrigues and S. Rosauero-Alcaraz, *The physics potential of a reactor neutrino experiment with Skipper CCDs: Measuring the weak mixing angle*, [2009.10741](#).
- [74] SOLID collaboration, *SoLid: A short baseline reactor neutrino experiment*, [2002.05914](#).
- [75] https://indico.cern.ch/event/773605/contributions/3494452/attachments/1897629/3131255/NuFact_NEON_190827_v5.pdf.
- [76] I. Avignone, F.T., R. Brodzinski, S. Dimopoulos, G. Starkman, A. Drukier, D. Spergel et al., *Laboratory Limits on Solar Axions From an Ultralow Background Germanium Spectrometer*, *Phys. Rev. D* **35** (1987) 2752.
- [77] CDMS collaboration, *Search for Axions with the CDMS Experiment*, *Phys. Rev. Lett.* **103** (2009) 141802 [[0902.4693](#)].
- [78] R. Bernabei et al., *Investigating pseudoscalar and scalar dark matter*, *Int. J. Mod. Phys. A* **21** (2006) 1445 [[astro-ph/0511262](#)].
- [79] SUPERCDMS collaboration, *Constraints on dark photons and axionlike particles from the SuperCDMS Soudan experiment*, *Phys. Rev. D* **101** (2020) 052008 [[1911.11905](#)].
- [80] *XCOM: Photon Cross Section Database*, 2010 (accessed June 11, 2020).
- [81] D. Aloni, C. Fanelli, Y. Soreq and M. Williams, *Photoproduction of Axionlike Particles*, *Phys. Rev. Lett.* **123** (2019) 071801 [[1903.03586](#)].
- [82] Y.-S. Tsai, *Axion Bremsstrahlung by an electron beam*, *Phys. Rev. D* **34** (1986) 1326.
- [83] Y.-S. Tsai, *Pair Production and Bremsstrahlung of Charged Leptons*, *Rev. Mod. Phys.* **46** (1974) 815.
- [84] R. H. Helm, *Inelastic and Elastic Scattering of 187-MeV Electrons from Selected Even-Even Nuclei*, *Phys. Rev.* **104** (1956) 1466.
- [85] PARTICLE DATA GROUP collaboration, *Review of Particle Physics*, *Phys. Rev. D* **98** (2018) 030001.
- [86] S. J. Brodsky, E. Mottola, I. J. Muzinich and M. Soldate, *LASER INDUCED AXION PHOTOPRODUCTION*, *Phys. Rev. Lett.* **56** (1986) 1763.
- [87] R. Chanda, J. F. Nieves and P. B. Pal, *Astrophysical Constraints on Axion and Majoron Couplings*, *Phys. Rev. D* **37** (1988) 2714.
- [88] F. Avignone, C. Baktash, W. Barker, F. Calaprice, R. Dunford, W. Haxton et al., *Search for Axions From the 1115-keV Transition of ^{65}Cu* , *Phys. Rev. D* **37** (1988) 618.
- [89] S. Dimopoulos, G. Starkman and B. Lynn, *Atomic Enhancements in the Detection of Axions*, *Mod. Phys. Lett. A* **1** (1986) 491.

- [90] M. Pospelov, A. Ritz and M. B. Voloshin, *Bosonic super-WIMPs as keV-scale dark matter*, *Phys. Rev. D* **78** (2008) 115012 [[0807.3279](#)].
- [91] A. Derevianko, V. Dzuba, V. Flambaum and M. Pospelov, *Axio-electric effect*, *Phys. Rev. D* **82** (2010) 065006 [[1007.1833](#)].
- [92] T. Donnelly and R. Peccei, *Neutral Current Effects in Nuclei*, *Phys. Rept.* **50** (1979) 1.
- [93] J. De Forest, T. and J. Walecka, *Electron scattering and nuclear structure*, *Adv. Phys.* **15** (1966) 1.
- [94] A. Barroso and N. C. Mukhopadhyay, *Nuclear axion decay*, *Phys. Rev. C* **24** (1981) 2382.
- [95] M. Krcmar, Z. Krecak, A. Ljubicic, M. Stipcevic and D. Bradley, *Search for solar axions using Li-7*, *Phys. Rev. D* **64** (2001) 115016 [[hep-ex/0104035](#)].
- [96] W. Haxton and K. Lee, *Red giant evolution, metallicity and new bounds on hadronic axions*, *Phys. Rev. Lett.* **66** (1991) 2557.
- [97] C. Hearty et al., *Search for the Anomalous Production of Single Photons in e^+e^- Annihilation at $\sqrt{s} = 29\text{-}\{GeV\}$* , *Phys. Rev. D* **39** (1989) 3207.
- [98] CAST collaboration, *Probing eV-scale axions with CAST*, *JCAP* **02** (2009) 008 [[0810.4482](#)].
- [99] M. Minowa, S. Moriyama, Y. Inoue, T. Namba, Y. Takasu and A. Yamamoto, *The Tokyo axion helioscope experiment*, *Nucl. Phys. B Proc. Suppl.* **72** (1999) 171 [[hep-ex/9806015](#)].
- [100] J. Jaeckel and M. Spannowsky, *Probing MeV to 90 GeV axion-like particles with LEP and LHC*, *Phys. Lett. B* **753** (2016) 482 [[1509.00476](#)].
- [101] J. W. Brockway, E. D. Carlson and G. G. Raffelt, *SN1987A gamma-ray limits on the conversion of pseudoscalars*, *Phys. Lett. B* **383** (1996) 439 [[astro-ph/9605197](#)].
- [102] G. G. Raffelt, *Astrophysical axion bounds diminished by screening effects*, *Phys. Rev. D* **33** (1986) 897.
- [103] G. G. Raffelt and D. S. Dearborn, *Bounds on Hadronic Axions From Stellar Evolution*, *Phys. Rev. D* **36** (1987) 2211.
- [104] A. Ayala, I. Domínguez, M. Giannotti, A. Mirizzi and O. Straniero, *Revisiting the bound on axion-photon coupling from Globular Clusters*, *Phys. Rev. Lett.* **113** (2014) 191302 [[1406.6053](#)].
- [105] P. Carena, O. Straniero, B. Döbrich, M. Giannotti, G. Lucente and A. Mirizzi, *Constraints on the coupling with photons of heavy axion-like-particles from Globular Clusters*, *Phys. Lett. B* **809** (2020) 135709 [[2004.08399](#)].
- [106] G. Lucente, P. Carena, T. Fischer, M. Giannotti and A. Mirizzi, *Heavy axion-like particles and core-collapse supernovae: constraints and impact on the explosion mechanism*, [2008.04918](#).

- [107] G. Raffelt, *Stars as laboratories for fundamental physics: The astrophysics of neutrinos, axions, and other weakly interacting particles*. University of Chicago Press, 1996.
- [108] N. Bar, K. Blum and G. D’Amico, *Is there a supernova bound on axions?*, *Phys. Rev. D* **101** (2020) 123025 [[1907.05020](#)].
- [109] S. Moriyama, M. Minowa, T. Namba, Y. Inoue, Y. Takasu and A. Yamamoto, *Direct search for solar axions by using strong magnetic field and x-ray detectors*, *Phys. Lett. B* **434** (1998) 147 [[hep-ex/9805026](#)].
- [110] Y. Inoue, Y. Akimoto, R. Ohta, T. Mizumoto, A. Yamamoto and M. Minowa, *Search for solar axions with mass around 1 eV using coherent conversion of axions into photons*, *Phys. Lett. B* **668** (2008) 93 [[0806.2230](#)].
- [111] CAST collaboration, *New CAST Limit on the Axion-Photon Interaction*, *Nature Phys.* **13** (2017) 584 [[1705.02290](#)].
- [112] J. Jaeckel, E. Masso, J. Redondo, A. Ringwald and F. Takahashi, *The Need for purely laboratory-based axion-like particle searches*, *Phys. Rev. D* **75** (2007) 013004 [[hep-ph/0610203](#)].
- [113] D. Cadamuro and J. Redondo, *Cosmological bounds on pseudo Nambu-Goldstone bosons*, *JCAP* **02** (2012) 032 [[1110.2895](#)].
- [114] M. Millea, L. Knox and B. Fields, *New Bounds for Axions and Axion-Like Particles with keV-GeV Masses*, *Phys. Rev. D* **92** (2015) 023010 [[1501.04097](#)].
- [115] P. F. Depta, M. Hufnagel and K. Schmidt-Hoberg, *Robust cosmological constraints on axion-like particles*, *JCAP* **05** (2020) 009 [[2002.08370](#)].
- [116] M. J. Dolan, T. Ferber, C. Hearty, F. Kahlhoefer and K. Schmidt-Hoberg, *Revised constraints and Belle II sensitivity for visible and invisible axion-like particles*, *JHEP* **12** (2017) 094 [[1709.00009](#)].
- [117] G. G. Raffelt, *Astrophysical axion bounds*, *Lect. Notes Phys.* **741** (2008) 51 [[hep-ph/0611350](#)].
- [118] EDELWEISS collaboration, *Searches for electron interactions induced by new physics in the EDELWEISS-III Germanium bolometers*, *Phys. Rev. D* **98** (2018) 082004 [[1808.02340](#)].
- [119] R. Essig, R. Harnik, J. Kaplan and N. Toro, *Discovering New Light States at Neutrino Experiments*, *Phys. Rev. D* **82** (2010) 113008 [[1008.0636](#)].
- [120] BOREXINO collaboration, *Search for solar axions emitted in the M1-transition of Li-7* with Borexino CTF*, *Eur. Phys. J. C* **54** (2008) 61.
- [121] BOREXINO collaboration, *Search for Solar Axions Produced in p(d, ³He)A Reaction with Borexino Detector*, *Phys. Rev. D* **85** (2012) 092003 [[1203.6258](#)].
- [122] A. Derbin, S. Bakhlanov, I. Dratchnev, A. Kayunov and V. Muratova, *Search for*

- axioelectric effect of 5.5 MeV solar axions using BGO detectors*, *Eur. Phys. J. C* **73** (2013) 2490 [[1306.4574](#)].
- [123] A. Derbin et al., *Search for axioelectric effect of solar axions using BGO scintillating bolometer*, *Eur. Phys. J. C* **74** (2014) 3035 [[1405.3782](#)].
- [124] PANDAX collaboration, *Limits on Axion Couplings from the First 80 Days of Data of the PandaX-II Experiment*, *Phys. Rev. Lett.* **119** (2017) 181806 [[1707.07921](#)].
- [125] CDEX collaboration, *Constraints on Axion couplings from the CDEX-1 experiment at the China Jinping Underground Laboratory*, *Phys. Rev. D* **95** (2017) 052006 [[1610.07521](#)].
- [126] MAJORANA collaboration, *New limits on Bosonic Dark Matter, Solar Axions, Pauli Exclusion Principle Violation, and Electron Decay from the Majorana Demonstrator*, *Phys. Rev. Lett.* **118** (2017) 161801 [[1612.00886](#)].
- [127] J. S. Lee, *Revisiting Supernova 1987A Limits on Axion-Like-Particles*, [1808.10136](#).
- [128] A. Bhusal, N. Houston and T. Li, *Searching for solar axions at the Sudbury Neutrino Observatory*, [2004.02733](#).
- [129] F. Calore, P. Carena, M. Giannotti, J. Jaeckel and A. Mirizzi, *Bounds on axion-like particles from the diffuse supernova flux*, [2008.11741](#).